ADVANCED FUNCTIONAL MATERIALS

www.afm-journal.de

Thioethyl-Porphyrazine/Nanocarbon Hybrids for Photoinduced Electron Transfer

Sandra Belviso, Andrea Capasso, Ernesto Santoro, Leyla Najafi, Francesco Lelj, Stefano Superchi, Daniele Casarini, Claudio Villani, Davide Spirito, Sebastiano Bellani, Antonio Esau Del Rio-Castillo, and Francesco Bonaccorso**

A novel pyrene-substituted thioethyl-porphyrazine (PzPy) and the formation of supramolecular assembly with nanocarbons demonstrating photoinduced electron transfer ability are designed. As revealed by spectroscopic and electrochemical studies, PzPy displays wide spectral absorption in the visible range, charge separation upon photoexcitation, as well as bandgap and highest occupied/lowest unoccupied molecular orbital (HOMO/LUMO) energy values, matching the key requirements of organic optoelectronic. Moreover, the presence of a pyrene moiety promotes attractive interactions with π-conjugated systems. In particular, theoretical calculations show that in the PzPy the HOMO and LUMO are localized on different positions of the molecule, i.e., the HOMO on the pyrene moiety and the LUMO on the macrocycle. Therefore, HOMO–LUMO excitation gives rise to a charge separation, preventing excitons recombination. Two kinds of noncovalent hybrid composites are prepared by mixing the PzPy with single-wall carbon nanotubes (SWNTs) and graphene nanoflakes (GNFs), respectively, and used for photocurrent generation through charge transfer processes between PzPy and nanocarbons. Photoconduction experiments show photocurrent generation upon visible light irradiation of both PzPy/SWNT and PzPy/GNF composites (0.78 and 0.71 mA W^{-1} at 500 nm, respectively), demonstrating their suitability for optoelectronic applications and light harvesting systems.

1. Introduction

The growing interest toward the development of new materials and technologies for optoelectronic application has fueled the research in organic materials due to their low-cost high-throughput film manufacturing by solution-processed techniques (spin casting, inkjet printing, roll-to-roll, and large-area deposition processes).[1–3] Moreover, organic films often features low-weight and high-flexibility, which are of interest in view of both scaling up prospective and device integrations, respectively.[1–5] Typically, photoactive organic films are based on electron donor–acceptor interactions, where photoexcitation of the donor promotes a charge separation accompanied by an electron transfer to the acceptor species.[1,5–7] The donors are usually semiconducting poly-aryl[6,7] and poly-heteroaryl[8] polymers or small molecules,[9,10] displaying high molar extinction coefficients ε ($>10^4$ M^{-1} cm^{-1}).[1–3] The acceptor systems are, instead, usually based on carbon

Dr. S. Belviso, Dr. E. Santoro, Prof. F. Lelj, Prof. S. Superchi, Prof. D. Casarini
Dipartimento di Scienze
Università degli Studi della Basilicata
via dell'Ateneo Lucano 10, 85100 Potenza, Italy
E-mail: sandra.belviso@unibas.it

Dr. S. Belviso, Prof. F. Lelj
LASCAMM
CR-INSTM Unità della Basilicata
85100 Potenza, Italy

Dr. A. Capasso, Dr. L. Najafi, Dr. S. Bellani, Dr. A. E. Del Rio-Castillo, Dr. F. Bonaccorso
Istituto Italiano di Tecnologia
Graphene Labs
Via Morego 30, 16163 Genova, Italy
E-mail: francesco.bonaccorso@iit.it

The ORCID identification number(s) for the author(s) of this article can be found under https://doi.org/10.1002/adfm.201705418.

DOI: 10.1002/adfm.201705418

Dr. L. Najafi
Dipartimento di Chimica e Chimica Industriale
Università degli Studi di Genova
Via Dodecaneso 3, 16163 Genova, Italy

Prof. C. Villani
Dipartimento di Chimica e Tecnologie del Farmaco
Università degli Studi di Roma "La Sapienza"
Piazzale Aldo Moro, 5, 00185 Roma, Italy

Dr. D. Spirito
Nanochemistry Department
Istituto Italiano di Tecnologia
Via Morego 30, 16163 Genova, Italy

Dr. F. Bonaccorso
BeDimensional Srl
Via Albisola 121, 16163 Genova, Italy

nanomaterials.[11] In particular, fullerene derivatives such as [6,6]-phenyl-C_{61}-butyric acid methyl ester (PCBM) have been widely used for this purpose.[12] More recently, carbon nanotubes (CNTs) have also been reported as acceptors,[13–15] and the use of graphene is rapidly raising too.[16–21] In particular, single-wall carbon nanotubes (SWNTs) have been proposed as acceptor material since they possess nanoscale diameter and large aspect ratio in combination with favorable electrical transport properties.[14,19] Furthermore, SWNTs show unique optoelectronic properties, electrochemical stability, and energy levels that can be suitably coupled to those of conjugated polymers with long-range charge transport properties to make efficient composites for optoelectronic devices.[19] Similarly, graphene has high electron and hole mobility at room temperature, with reported values exceeding 15 000 $cm^2\ V^{-1}\ s^{-1}$.[20–22] Graphene is also electrochemically stable, with a very high specific surface area (≈2630 $m^2\ g^{-1}$), surpassing that of both SWNTs and graphite.[23,24] Moreover, graphene has an optical transmittance over the visible range of 97.7%,[25] and its work function (≈4.5 eV)[26] can be matched to the energy levels of organic donor materials.[22] Moving from these motivations, both SWNTs and functionalized graphene have been used as electron acceptors in combination with conjugated polymer donors, such as poly(3-octylthiophene), or poly(*p*-phenylenevinylenes), and poly(3-hexylthiophene),[14,19,27,28] especially in organic bulk heterojunction (BHJ) solar cell devices.[19]

Among the nonpolymeric donors a prominent role is occupied by tetrapyrrole macrocycles such as porphyrins[29] and phthalocyanines,[29,30] which, since the first organic solar cell reported by Tang in 1986 based on Cu-phthalocyanine,[31] have been widely used as p-type photoelectron donor dyes transferring charges to an n-type acceptor system.[32–35] Recently, photoactive hybrid materials constituted by a tetrapyrrolic macrocycle donor linked to a nanocarbon acceptor (e.g., CNTs) have been reported,[30,36,37] with the linkage occurring by either covalent bonding[38–43] or supramolecular interactions with the CNT surface.[44–62] The latter is the most promising approach, avoiding chemical modification of the CNT surface, which determines a modification of the CNT sp^2 network and, consequently, of its electronic structure.[63] Noncovalent interactions between the tetrapyrrole dye and the CNT are usually mediated by pyrene units, which interact with the aromatic surface of the nanocarbon through π–π stacking bonding.[51,52,54–56] Notably, in the existing literature the pyrene is not directly linked to the macrocycle, but it is, instead, linked through an alkyl chain spacer[52,55] or benzofused to the macrocycle itself.[62] Recently, photoactive hybrid materials composed by porphyrins and phthalocyanines with graphene[64–70] and its derivatives (e.g., graphene oxide[71] and reduced graphene oxide[72,73]) have also been described. In some of these examples,[64–66] the supramolecular interactions between the macrocycle and graphene[74] are mediated by the presence of a pyrene unit linked to the macrocycle through an alkyl chain spacer. These results highlight the fact that nanoassemblies of tetrapyrroles with either CNTs or graphene represent promising materials for the development of novel optoelectronic devices.

Seeking for new types of tetrapyrrole donors, there is a huge potential in porphyrazines,[75,76] which can be considered as structural hybrids of porphyrins and phthalocyanines, but have never been investigated for photocurrent generation so far. In particular, thioalkyl porphyrazines, having thioethereal moieties at the β-position of the macrocycle, are rather interesting. In fact, the presence of sulfur atoms imparts outstanding optical and electrochemical properties[77–83] to these compounds, promoting coordination sites out and above the molecular plane and favoring the presence of columnar discotic liquid-crystalline mesophases.[77–80] This is a relevant feature because highly ordered materials such as liquid crystals assist both exciton and charge carrier mobilities.[1,84–86] One of the key research effort in optoelectronic devices is devoted to increase the spectral response of the photoactive layer, obtaining panchromatic light absorbers, which can be ideal candidates for both photodetecting and energy harvesting applications. In the UV–visible light range porphyrins and phthalocyanines display narrow and strong ($\varepsilon \approx 3$–$6 \times 10^5\ M^{-1}\ cm^{-1}$) absorption bands at about 400 and 680 nm, respectively, but only 10% of the overall absorption lies in the 450–600 nm range, where the solar emission reaches its maximum.[29,87] On the contrary, the absorption spectrum of thioalkyl porphyrazines displays bands having lower ε (≈ 1–$5 \times 10^4\ M^{-1}\ cm^{-1}$), but being much wider in the 300–800 nm range.[78] A higher total absorbance then results in the wavelength range corresponding to the maximum of the solar emission spectrum.[81,88,89]

Recently, some of us prepared several aryl- and arylethynyl-substituted thioalkyl-porphyrazines, in which both electron-donating and electron-withdrawing groups strongly perturbed the molecular charge distribution.[83] Computational density functional theory (DFT) and time-dependent density functional theory (TDDFT) studies indicated that while in symmetrical porphyrazines both the highest occupied molecular orbital (HOMO) and the lowest unoccupied molecular orbital (LUMO) are localized on the macrocycle, in compounds with electron-donating groups the HOMO is localized on the aryl substituent and LUMO on the macrocycle, while the opposite holds in the presence of electron-withdrawing groups.[83] In the aryl- and arylethynyl-substituted systems, the macrocycle then displays an ambivalent character, behaving both as electron acceptor and electron donator depending on the substituents, giving rise to an unconventional "push–pull" system suitable for nonlinear optics.[90] These features can also play a relevant role in photoactive materials because the presence of charge transfer HOMO–LUMO transitions and the location of these orbitals on different moieties of the molecules can, in principle, hinder exciton recombination enhancing its lifetime, making these compounds promising electron donors. Moreover, all these aryl- and arylethynyl-substituted porphyrazines show HOMO and HOMO–LUMO bandgap energies compatible with nanocarbons as acceptors.[91]

Taking into account the charge transfer properties of these compounds and the possibility to functionalize the porphyrazine macrocycles, we designed and prepared a novel pyrene-substituted thioalkyl-porphyrazine **PzPy** (**Scheme 1**) to be exploited for photocurrent generation. In this compound, a macrocycle, which is a strong light absorber, and a pyrene unit, which is able to interact with the nanocarbons, are present simultaneously. Moreover,

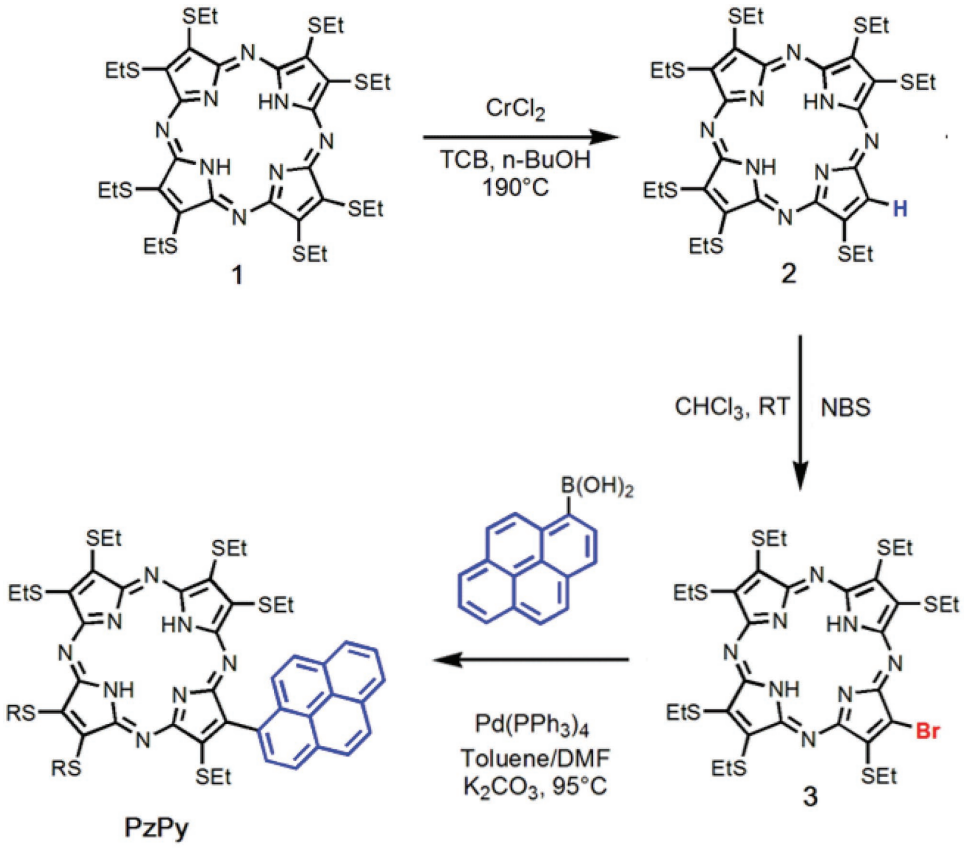

Scheme 1. Synthesis of pyrene-substituted thioethyl-porphyrazine **PzPy**.

the direct bond between the macrocycle and pyrene moieties can, in principle, allow an electron exchange between them, promoting a charge separation upon photoexcitation likewise the above-mentioned aryl-substituted porphyrazines.[83] For these reasons, this compound is particularly suited for the formation of nanohybrids with CNTs and graphene. The preparation of **PzPy**/nanocarbon hybrids, the study of the supramolecular interactions within the composites, and the results of photoconduction experiments are reported herein. We prepared and fully characterized two different noncovalent hybrid composites by mixing the **PzPy** with either SWNTs or graphene nanoflakes (GNFs). We have then fabricated photodetectors, which show photocurrent generation upon visible light irradiation reaching 0.78 and 0.71 mA W^{-1} at 500 nm, for **PzPy**/SWNT and **PzPy**/GNF composites, respectively. To the best of our knowledge, these systems are the first example of hybrid composed by nanocarbons and alkyl porphyrazines and the first case in which graphene and pyrene-substituted tetrapyrroles nanohybrids are used to assemble photoactive devices. In fact, the only two examples reported in literature so far concern the use of graphene and phthalocyanine poly(*p*-phenylene vinylene oligomers,[69,70] contrary to our case in which single molecules of tetrapyrrole are used. Moreover, the use of graphene as electron acceptor in tetrapyrrole-based optoelectronics represents a breakthrough for the development of novel organic optoelectronic devices.

2. Results and Discussion

2.1. Synthesis and Structural Characterization

The pyrene-substituted thioethyl porphyrazine **PzPy** is prepared in a three-step procedure starting from the parent symmetrically substituted thioethyl porphyrazine **1** (Scheme 1).[92] The first step is a hydrogen replacement of one alkylsulfanyl tail leading to the nonsymmetrical β-H-substituted porphyrazine **2**.[81] Such approach affords a very clean reaction, easy purification procedures, yielding a nonsymmetrically substituted product. The subsequent bromination of **2** leads to the bromo derivative **3**,[82] which, through Pd-catalyzed Suzuki[93,94] coupling reaction,[79,83] provides the pyrene-substituted thioethyl porphyrazine **PzPy** in 45% yield.

Supramolecular interactions between aromatic systems and nanocarbons are usually determined by noncovalent π–π interactions[68,95] which, being highly directional,[96] are strictly dependent on shape and mutual orientation of the interacting molecules. Therefore, **PzPy** is fully characterized for its structural, conformational, and stereochemical features. The **PzPy** stereochemical aspects are particularly interesting because in this molecule hindered rotation around the pyrene-macrocycle bond is expected to induce a twist of the pyrene moiety from the porphyrazine plane and then the presence of atropisomerism. This structural feature is relevant for the possible interactions with SWNTs. In fact, the presence of an axially chiral

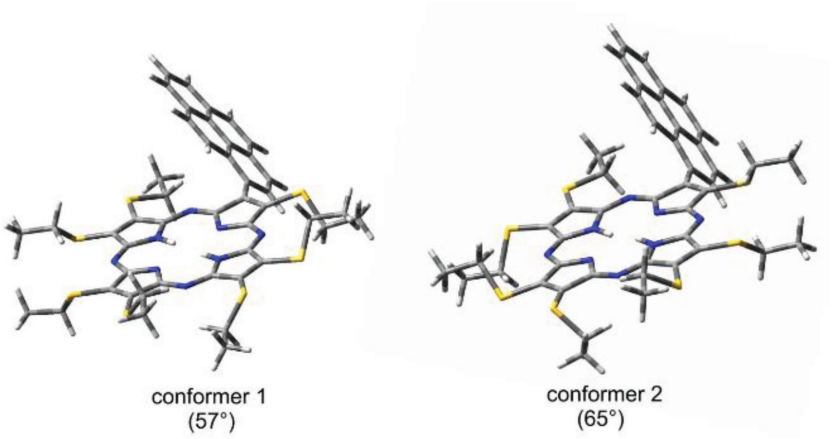

Figure 1. Computed (DFT/M06/6-311G(d,p)/CH_2Cl_2) most stable conformers of **PzPy**.

structure in **PzPy** could favor the interaction with semiconducting chiral CNTs, which are known to be optically resolved by chiral biaryls and bis-porphyrins.[97–102] Besides, the **PzPy**-twisted arrangement should not impair the interaction with the 2D graphene structure, given that attractive arene–arene interactions are often edge-to-face and offset stacked rather than face-to-face stacked.[103,104]

Density functional theory computations at M06/6-311G(d,p) level of theory, taking into account the solvent environment by IEFPCM solvation model,[105,106] clearly revealed the twist of the pyrene ring in the two most stable conformers, having a dihedral angle of 57° and 65° between the pyrene and macrocycle, respectively (see **Figure 1** and Table S1 in the Supporting Information). An arene–arene rotational barrier of 23.44 kcal mol^{-1} was also calculated. Experimental measurements by variable temperature nuclear magnetic resonance (NMR) and variable temperature high-performance liquid chromatography (HPLC) analyses[107–109] provided a rotational barrier of 22.0 ± 0.1 kcal mol^{-1},[110] i.e., lower than that obtained by calculations, a value which does not allow isolation of the single enantiomers at room temperature.[111,112] However, even if **PzPy** cannot be isolated in its enantiomeric forms at room temperature, its molecular axial chirality is nevertheless important because it can also favor the interaction with semiconducting racemic chiral nanotubes.

2.2. Spectroscopic and Electrochemical Study

The electronic properties of **PzPy** are investigated by experimental and theoretical analyses of its UV–vis spectrum. In **Figure 2** is reported the experimental UV–vis spectrum of **PzPy** in CH_2Cl_2 together with those of the parent porphyrazine **1** and of 1-pyrene boronic acid, taken as a model of unconjugated pyrene chromophore. The UV–vis spectrum of **PzPy** shows the typical features of nonaggregated "free-base" thioalkyl-porphyrazines, displaying a $Q_x(0, 0)$ band at 709 nm (14 104 cm^{-1})[89] and a broad $Q_y(0, 0)$ band at 640 nm (15 625 cm^{-1}),[89] a Soret band near 350 nm (28 571 cm^{-1}),[89] and in between a band at 513 nm (19 493 cm^{-1}) associated with $n_{sulfur} \rightarrow \pi^*$ transitions.[83,88,89] Moreover, an absorption band peaked at 277 nm (44 052 cm^{-1}), corresponding to one of the typical bands of the pyrene chromophore,[113,114] is clearly visible. Such band is allied to a long-axis polarized pyrene transition and the fact that it appears less resolved than in unconjugated pyrene indicates an electronic connection between the two aromatic moieties.[113] The spectral comparison with the parent unsubstituted porphyrazine **1** (Figure 2) evidences a marked increase of the Soret band, which cannot be simply ascribed to a contribution of the underneath characteristic pyrene features located at 330 and 345 nm (30 303 and 28 985 cm^{-1}),[113] which are far less intense, but can be associated with intramolecular delocalization.[113]

To get further insight into the electronic structure of **PzPy**, a TDDFT computational investigation is carried out to provide an interpretation of the UV–vis spectral features. The UV–vis computed spectrum at the M06/6-311G(d,p)/CH_2Cl_2 level of theory in the 23 500–12 500 cm^{-1} (435–800 nm) range is characterized by 12 transitions $S_0 \rightarrow S_n$ (n = 1, 12) in the case of conformers 1 and 2 (Figure 1). Conformer 2 shows transitions hypsochromically shifted compared to conformer 1 (see **Figure 3**). **Figure 4** reports the main molecular orbital (MO) levels composition and the corresponding orbital energies for conformer 1, while a full interpretation of the MO's electronic transitions allied to the main spectral features is reported in the Supporting Information. As inferred from Table S3 in the Supporting Information, almost all the transitions have multideterminant character with at least two configurations contributing to their composition. As a general trend, all the transitions in the aforementioned range are generated by excitations between occupied orbitals in the range

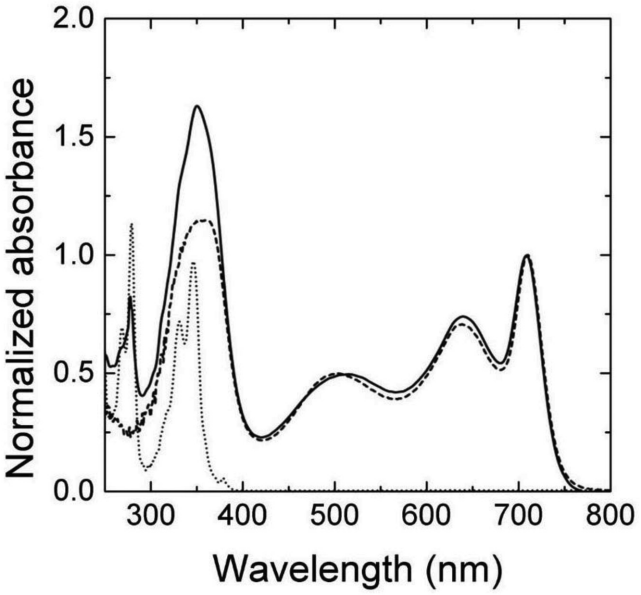

Figure 2. Experimental (CH_2Cl_2) UV–vis spectra for **PzPy** (solid line), porphyrazine **1** (dashed line), and 1-pyrene boronic acid (dotted line).

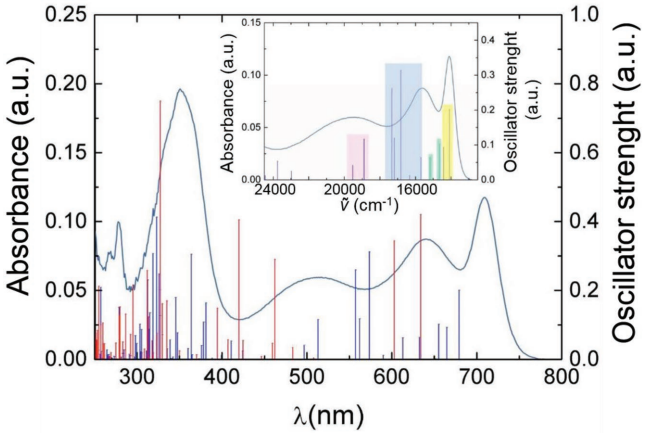

Figure 3. TD-DFT Kohn–Sham first 75 singlet states computed at the M06/6-311G(d,p)/CH_2Cl_2 level of theory for conformers 1 and 2 (blue and red sticks, respectively); continuous line: UV–vis **PzPy** spectrum in CH_2Cl_2. Inset: Singlet states in the 23 500–12 500 cm^{-1} (425–800 nm) range for conformer 1. Energies of the transitions in the inset have been bathochromically shifted by 0.077 eV (621 cm^{-1}). Shaded areas have the same coloring as shaded areas on the occupied MO levels involved in the transitions shown in Figure 4. All reported excitations encompass LUMO and LUMO+1 ("pale red" shaded same as Figure 4) and their composition is detailed in Table S3 in the Supporting Information.

HOMO–HOMO-5 and empty ones LUMO and LUMO+1, these two being localized on the porphyrazine core. In particular, S_1 and S_2 involve excitations from HOMO to LUMO and LUMO+1. The composition of these three MO levels gives to the transitions a well-defined charge transfer (pyrene → porphyrazine) character. This process, which determines upon excitation the separation of electrons and holes on different parts of the molecule, can be relevant for both the exciton formation and lifetime. The presence of charge transfer HOMO–LUMO transitions and the location of these orbitals on different moieties of the molecules, reducing the kinetics of the radiative relaxation processes, prevent exciton recombination, thus making this compound promising dye as photoactive material for optoelectronics.

The UV–vis spectrum of **PzPy** is also recorded in dimethylformamide (DMF) (Figure S5 in the Supporting Information), the solvent chosen for the preparation of nanocomposites with SWNTs and GNFs. The spectrum recorded in anhydrous DMF is markedly different from the one in CH_2Cl_2, rather closely resembling that of a thioalkyl porphyrazine metal complex[83] with a single Q band located at 665 nm (15 037 cm^{-1}) (Figure S6 in the Supporting Information). This effect, also observed in substituted phthalocyanines,[55,115,116] can be ascribed to a deprotonation of the macrocycle inner cavity which produces

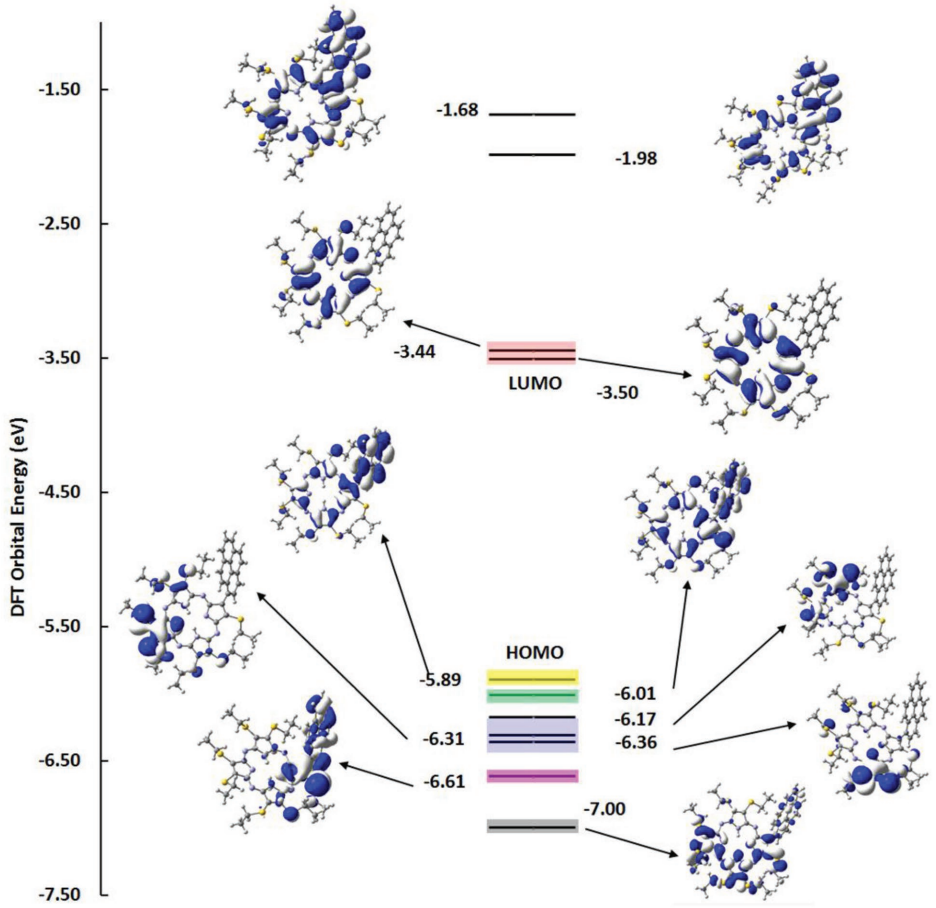

Figure 4. DFT Kohn–Sham orbital energies at the M06/6-311G(d,p)/CH_2Cl_2 level of theory involving the excitations contributing to the states in the 23 000–12 500 cm^{-1} (435–800 nm) range computed for conformer 1 of **PzPy**. Shaded areas have the same coloring as the transitions in the spectrum of Figure 3, inset, indicating the MOs from where transitions start. Surface contours are drawn at 0.02(e au^{-3})$^{1/2}$.

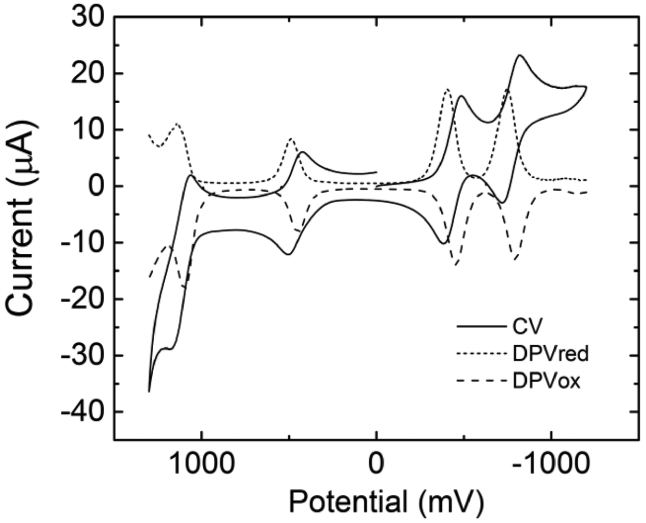

Figure 5. Cyclic voltammogramm and differential pulse voltammogramms of **PzPy** in CH_2Cl_2.

more symmetric anionic structures having D_{4h} symmetry like the metal complexes.[117] This is also confirmed by basic titration of phthalocyanines, which shows a pH-dependent transition from the typical "free-base" UV–vis spectrum to that of mono- and dianionic species, both identical to those of the corresponding metal complexes.[118,119] Contrary to what is reported in literature,[55,117] our understanding is that the macrocycle deprotonation cannot be ascribed to DMF, which is not basic enough (pK_b 15.2)[120] to remove the inner pyrrolic protons (pK_a 12.5),[118,119] but to dimethylamine traces (pK_b 3.27)[121] usually present as impurities in commercial DMF.[122] Experimental and computational studies reported in the Supporting Information further confirmed such hypothesis. Notably, a typical "free-base" UV–vis spectrum, similar to that obtained in CH_2Cl_2, is instead observed in nonanhydrous DMF (Figure S5 in the Supporting Information), where the water present in the solvent competes as acid with the porphyrazine in the acid–base equilibrium with the amine. In summary, the shape of the **PzPy** UV–vis spectrum in DMF depends on the water content of the solvent: a complex-like spectrum appears in anhydrous DMF, while a spectrum due to superimposition of anionic and "free-base" species appears in a wet solvent, as demonstrated by the presence of three isosbestic points at 446, 620, and 690 nm (Figure S5 in the Supporting Information).[55]

The cyclic voltammetry (CV) and differential pulse voltammetry (DPV) measurements of **PzPy** in CH_2Cl_2 are reported in **Figure 5** and the electrochemical data for both solvents are collected in **Table 1**. The redox behavior of **PzPy** appears as the typical one of thioalkyl-porphyrazines. In fact, two sequential one-electron reduction processes are present in the cathodic region, which can be assigned to the formation of a porphyrazine π-anion radical and a porphyrazine dianion, respectively.[83,123,124] The redox processes in CH_2Cl_2 are characterized by a cathodic peak and its anodic counterpart displaying half-wave potentials $E_{1/2}(\Delta E_p)$ = –0.900 V (0.096) and $E_{1/2}(\Delta E_p)$ = – 1.232 (0.095) (vs Fc/Fc^+, used as internal standard), respectively. Both processes can be considered as quasireversible because the conditions for the reversibility are not rigorously fulfilled (as inferred from $\Delta E_p = |E_a - E_c|$ values). Furthermore, CV of compound **PzPy** shows a quasireversible oxidation wave with $E_{1/2}(\Delta E_p)$ = +0.657 V (0.108) (vs Fc/Fc^+). HOMO and LUMO energies obtained from electrochemical data are reported in Table 1, by assuming the energy level of ferrocene/ferrocenium at –4.8 eV.[125–127] The HOMO energies are also estimated according to a recent procedure, taking into account solvation and electrode surface effects.[128] As inferred from the electrochemical data in DMF (Table 1), strong anodic shifts for all the potential values with respect to CH_2Cl_2 are observed. In this case, it must be recalled that the potential values can be affected not only by the solvent but also by the presence of anionic species together with the "free base" porphyrazine (vide supra). However, these factors are expected to have a minor influence because only small potential changes are observed retaining electrochemical data in both anhydrous and not anhydrous DMF. Notably, the HOMO and LUMO energy values make **PzPy** suitable for fabrication of BHJ cells with nanocarbons as acceptors. In fact, with acceptors such as PCBM, SWNT, and graphene, having work functions[26,129–131] in the –4.3 to –4.9 eV range, donors with HOMO energy values lower than –5.20 eV and a bandgap energy range of 1.30–1.80 eV are required.[132]

The DFT-computed values for the HOMO and LUMO energies at the M06/6-311G(d,p) level of theory in CH_2Cl_2 are –5.85 and –3.48 eV, respectively, and –5.87 and –3.50 eV in DMF. These data are in good agreement with values calculated from experimental ones. Notably, the HOMO–LUMO transition also retains a charge transfer character in DMF (see Figure S9 in

Table 1. Summary of the peak potentials of **PzPy** $E_{1/2}$ ($\Delta E_p = |E_a - E_c|$) (volts vs Fc/Fc^+).

Solvent[a]	Technique	Oxidation	Reduction		E_{HOMO}			E_{LUMO}	
			I	II	Experimental[b]	Experimental[c]	Computational[d]	Experimental[b]	Computational[d]
CH_2Cl_2	(CV)	0.657 (0.108)	–0.900 (0.096)	–1.232 (0.095)	–5.46	–5.52 ± 0.18	–5.85	–3.90	–3.48
	$(DPV)_{ox}$	0.648	–0.902	–1.240	–5.45	–5.51 ± 0.18		–3.90	
	$(DPV)_{red}$	0.650	–0.896	–1.234	–5.45	–5.51 ± 0.18		–3.90	
DMF[e]	(CV)	n.d.	–0.738 (0.064)	–1.130 (0.060)	n.d.	n.d.	–5.87	–4.06	–3.50
	$(DPV)_{ox}$	0.716	–0.752	–1.152	–5.52	–5.60 ± 0.18		–4.05	

[a]Measured 10^{-3} M solution at a glassy carbon working electrode; [b]Values (eV) referred to first oxidation and first reduction, and calculated assuming the energy level for the ferrocene at –4.8 eV (see ref. [126]); [c]Values (eV) obtained by the equation $E_{HOMO} = -(1.4 \pm 0.1) \times q \times V_{CV} - (4.6 \pm 0.08)$ (see ref. [128]); [d]Computations in CH_2Cl_2 and DMF by PCM solvation model as described in the Experimental Section and at the M06/6-311G(d,p) level of theory; [e]Anhydrous DMF solvent.

the Supporting Information). The long-range corrected xc-functional CAM-B3LYP gives values of –6.62 and –2.77 eV in CH_2Cl_2, suggesting that the hypsochromic shift in the low energy part of the absorption spectrum is due to a too large HOMO–LUMO energy gap engendered by this xc-functional.

2.3. Hybrid PzPy/Nanocarbons

PzPy is used to prepare noncovalent bonded nanohybrid composites with two classes of nanocarbons, SWNTs and graphene. As described in the Experimental Section, commercially available SWNTs (diameter range of 0.7–1.1 nm) are characterized and then dispersed in DMF, and subsequently mixed with **PzPy** for the composites realization. DMF is preferred with respect to *N*-methyl-2-pyrrolidone, one of the best solvent for the dispersion of nanocarbons,[133,134] for its lower boiling point (152 °C vs 202 °C), which helps its removal by evaporation during the device preparation.[135] Raman spectroscopy is used for the nanotubes structural characterization and to ascertain the batch composition (see discussion in the Supporting Information). The Raman analysis performed with an excitation wavelength of 532 nm confirms that the SWNTs batch is composed, at least, by a mixture of nanotubes, with chiralities (10,3), (9,2), (7,6), and (7,5), which are resonant to 532 nm excitation wavelength.[136]

Electron microscopy is used to study the interaction between SWNTs and **PzPy**. **Figure 6**a reports a scanning electron microscope (SEM) image taken on pristine SWNTs deposited onto a Si/SiO_2 substrate. The SWNTs appear strongly entangled and forming bundles. By comparison, the **PzPy**/SWNT nanohybrid (Figure 6c) evidences an intermixed structure between the composite materials. The transmission electron microscopy (TEM) image of SWNTs in Figure 6b shows the presence of large aggregates of nanotubes with length in the order of hundreds of nanometers (see the Supporting Information for statistical analysis). The comparison with the TEM image of the nanohybrid composite (Figure 6d) suggests the interaction between **PzPy** and SWNTs. In fact, the nanotubes appear here debundled for the effect of π–π interactions between the **PzPy** and the SWNT sidewalls, which overcome nanotube–nanotube van der Waals attraction.[137] In Figure 6d the presence of a molasses-type film of **PzPy** covering the nanotubes is also clearly visible, further confirming the expected strong supramolecular interactions between the two materials.

To investigate more in details the **PzPy**/SWNT nanohybrid, UV–vis–NIR absorption and fluorescence spectroscopies are performed. The spectrum of the pristine SWNTs (**Figure 7**a) confirms the presence of different SWNTs chiralities.[100] The steady-state absorption spectroscopic measurements of **PzPy**/SWNT nanocomposites show some diagnostic changes in the macrocycle absorption features upon nanotubes enrichment (Figure 7b). The SWNTs dispersion contributes to the increase in optical density, especially in the blue region of the spectra, giving rise to an increase of the 350 nm absorption, related to the porphyrazine Soret band, with respect to the Q bands. Moreover, a splitting and broadening of the Soret band is observed, revealing interaction between the macrocycle and the added SWNTs.[63,98] Upon excitation, compound **PzPy** displays emission spectra significantly more intense than **1**, lacking the pyrene moiety.

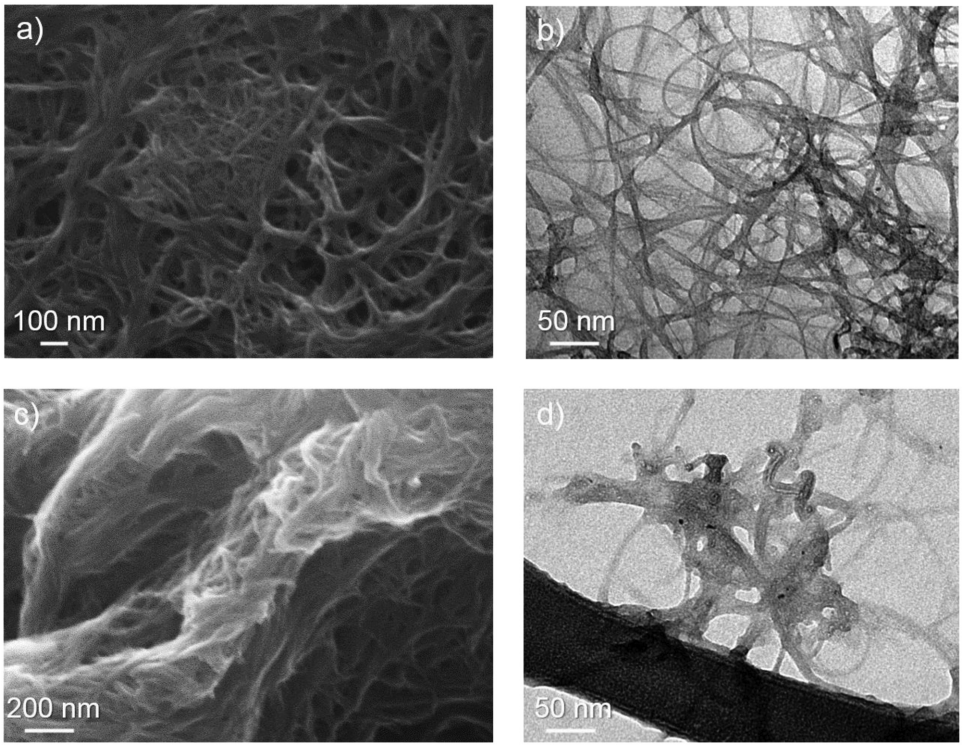

Figure 6. Electron microscopy of SWNTs and **PzPy**/SWNT nanohybrid. SEM images of a) SWNTs and c) **PzPy**/SWNT nanohybrid deposited on a Si/SiO_2 substrate. TEM images of b) SWNTs and d) **PzPy**/SWNT nanohybrid drop cast from a DMF solution on a lacey carbon TEM grid.

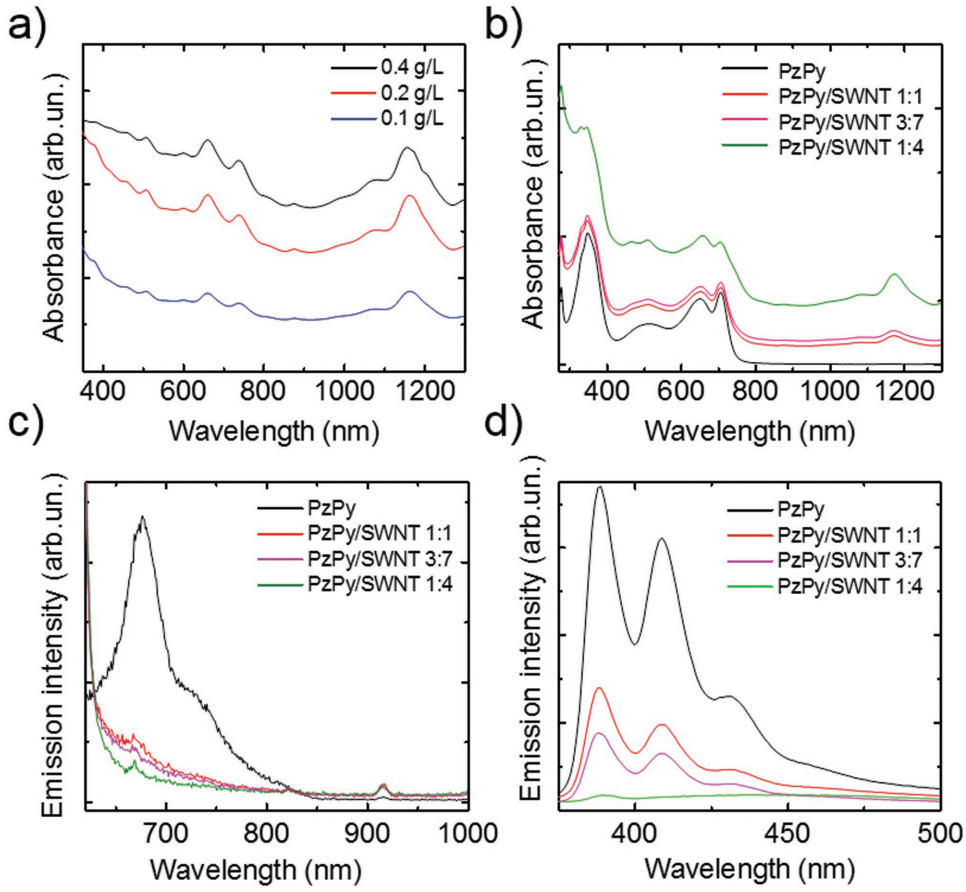

Figure 7. UV–vis absorption spectra of DMF dispersions of a) SWNTs and b) **PzPy**/SWNT nanohybrids in DMF at various weight ratios (see the Experimental Section). Emission spectra of **PzPy**/SWNT nanohybrids with excitation at c) 610 nm and d) 350 nm.

Analysis of emission spectra at two different excitation wavelengths clearly shows that addition of SWNTs to the porphyrazine dispersion gives rise to a strong quenching of the macrocycle fluorescence (Figure 7c,d). Exciting at 350 nm (Figure 7d), the emission bands allied to the pyrene chromophore proportionally decrease upon SWNT addition. On the contrary, at 610 nm excitation wavelength (Figure 7c), the fluorescence ascribed to the macrocycle immediately drops, completely quenching at a 1:1 **PzPy**/SWNT weight ratio. These effects suggest the occurrence of excited-state events such as electron transfer and energy transfer,[45,54] which highlight the presence of a porphyrazine-SWNT interaction. The preparation of nanocomposite of **PzPy** with GNFs (**PzPy**/GNF) is also carried out. Graphene nanoflakes are obtained by ultrasonication of pristine graphite[133,138] and centrifugation in DMF (see the Experimental Section for details). The GNFs sample is characterized by Raman spectroscopy, a fast and nondestructive technique used to identify number of layers, defects, doping, disorder, and possible chemical modifications.[139,140] The Raman spectrum of the obtained GNFs (**Figure 8**) shows the typical D, D', G, and 2D bands of graphene. See the Supporting Information for the physical description of these Raman modes. The 2D peak position is at ≈2696 cm^{-1} and its full width at half-maximum is ≈60 cm^{-1}. The $I(2D)/I(G)$ intensity ratio ranges from 0.6 to 0.7. This is consistent with the samples being a combination of single-layer graphene and few-layer graphene flakes.[141] The Raman spectra show significant D (≈1345 cm^{-1}) and D' (≈1615 cm^{-1}) peaks intensity, with $I(D)/I(G)$ ranging from 0.9 to 1.3. This is attributed to the edges of submicrometer flakes[142] rather than to the presence of a large amount of structural defects. Indeed, if a large amount of defects were present in the basal plane of graphene the G (1582 cm^{-1}) and D′ peak should merge into a broader band,[143] which is not the case for the spectra of our dispersions.[141]

The **PzPy**/GNF composites are prepared by mixing and stirring the porphyrazine and the GNFs dispersions in DMF at different weight ratios. The **PzPy**/GNF composite is studied by electron microscopy. **Figure 9**a shows a SEM image of GNFs deposited onto a Si/SiO_2 substrate: the GNFs cluster in stacks forming a rather uniform film. When isolated, as in the TEM image in Figure 9b, it is possible to evaluate their size distribution in lateral size peaking at 150 nm, see Figure S11 in the Supporting Information for the statistical analysis. The SEM image in Figure 9c and TEM image in Figure 9d provide an insight into the morphology of the **PzPy**/GNF nanohybrid, where the GNF appears as a **PzPy** scaffold uniformly distributed.

Comparison of the Raman spectra of the porphyrazine and the graphene composite evidences a difference in the signal in the 900–1100 cm^{-1} range allied to the porphyrazine macrocycle (Figure S10 in the Supporting Information). The comparison with the pristine graphene shows that in the composite the

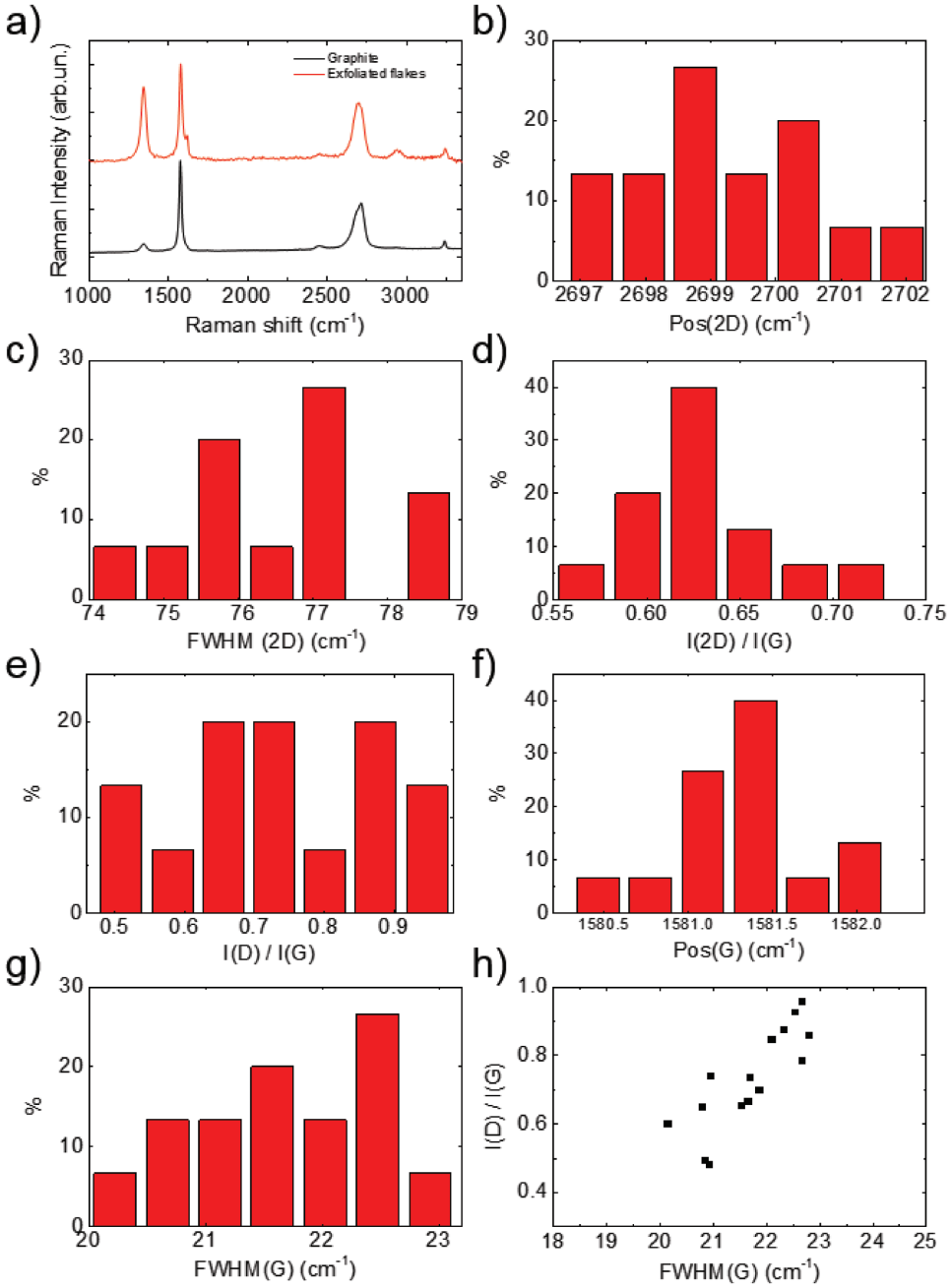

Figure 8. Raman spectra and statistics of the GNF drop cast from a DMF dispersion onto a Si/SiO_2 substrate (excitation at $\lambda = 532$ nm).

I(D)/I(G) and I(D')/I(G) ratios increases, indicating an increment of sp^3-hybridized carbon atoms, which may be related with the presence of the alkyl chains of the **PzPy** molecules.

The absorption spectra of the composites do not show any appreciable changes with respect to the spectra of the individual components (**Figure 10**b). In fact, maxima of the UV–vis region for the **PzPy**/GNF DMF dispersions are identical with the one of **PzPy** in DMF.

On the contrary, fluorescence experiments for **PzPy**/GNF hybrid exciting at two different wavelengths show that, increasing the graphene/porphyrazine ratio, the fluorescence of the macrocycle is proportionally reduced. It reveals that in this case also an energy transfer process between the two species occurs, confirming the hybrid formation (Figure 10c,d). These quenching experiments show that in the hybrid with nanotubes a more efficient energy transfer process occurs with respect to the one with graphene. In fact, by comparison of Figures 7c and 10c it can be noticed that, while a complete emission quenching is observed in a 1:1 **PzPy**/SWNT hybrid, a higher percentage of GNFs with respect to the **PzPy** is necessary to obtain the same effect. This suggests a stronger interaction between the **PzPy** and SWNT with respect to that between **PzPy** and GNF. In fact, the computed molecular conformations of the **PzPy** porphyrazine present a dihedral angle between the two aryl moieties,

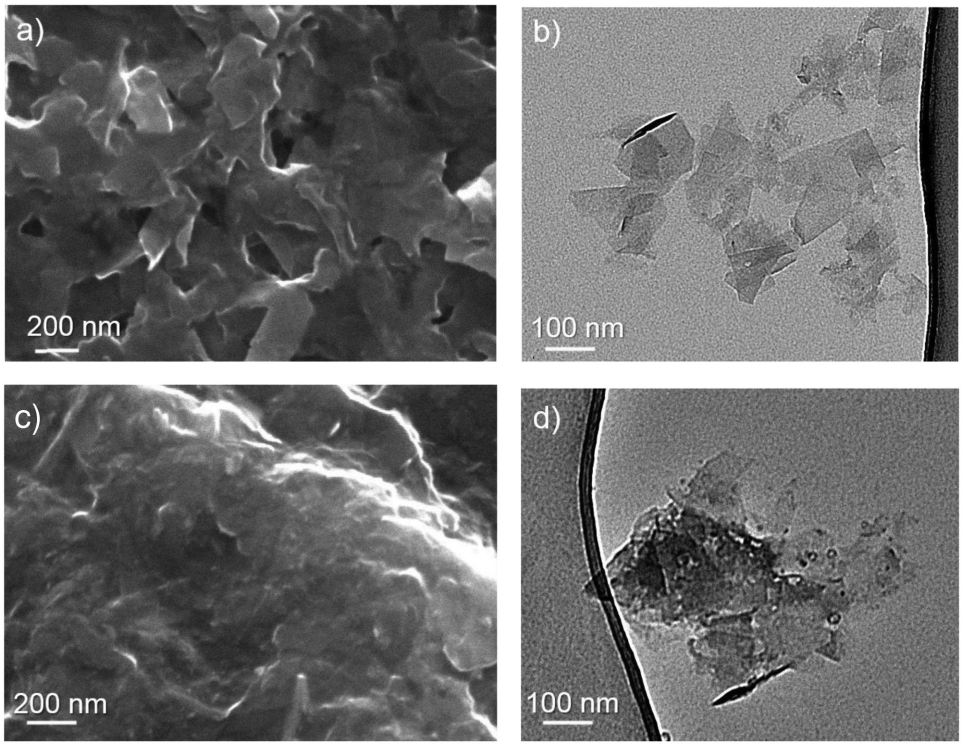

Figure 9. Electron microscopy of GNF and **PzPy**/GNF. SEM images of a) GNF and c) **PzPy**/GNF nanohybrid deposited on a Si/SiO_2 substrate. TEM images of b) GNF and d) **PzPy**/GNF nanohybrid drop cast from a DMF dispersion on a lacey carbon TEM grid.

which makes the compound suitable to wrap the SWNT, thus allowing π–π interactions with both the aromatic units (**Figure 11**). A similar effect has recently been observed in molecular dynamics simulation of interactions between SWNTs and chiral binaphthyl dendrimers.[144] On the contrary, the planar structure of graphene prevents the simultaneous interaction of both the macrocycle and the pyrene moieties.

2.4. Photoconduction Experiments on PzPy Nanohybrids

To test the optoelectronics properties of the as-synthesized **PzPy** nanohybrids and measure their photoconductivity under visible light illumination, we fabricated photodetectors by depositing films of the pristine **PzPy**, the composite **PzPy**/GNF, and **PzPy**/SWNT on interdigitated gold electrodes through drop casting method (see Device Fabrication and Measurement in the Experimental Section). Pristine GNF and SWNT films were also tested; however the resulting devices were electrically shortened (resistance between 100 and 1000 Ω), thus yielding high dark current densities without any photoresponse, therefore their data are not reported in the following discussion.

The device architecture is depicted in **Figure 12**a. Under monochromatic illumination at a wavelength of 500 nm (with intensity of 0.39 mW cm^{-2}), the **PzPy** film shows a linear photocurrent in the range 0–1 V, reaching 20 nA at 1 V bias voltage. The **PzPy**/GNF device presents a higher photocurrent, with respect to the **PzPy** one, throughout the whole range (Figure 12c). The I/V curve is linear between 0 and ≈0.4 V, where a steep increase occurs, bringing the current up to 92 nA at 1 V. In the case of the **PzPy**/SWNT device, the overall I/V curve shape is analogous but with a smaller current (13.5 nA vs 18.0 nA) at a bias voltage of 0.2 V. The two curves cross at 36.5 nA for 0.54 V. However, beyond 0.55 V, the current increase up to 112 nA at 1.0 V. Concerning the responsivity (Figure 12d), the photodetector with **PzPy**/GNF as active material has a 2.6-, 3.5-, and 4.8-fold increase at 0.2, 0.6, and 1.0 V, respectively, compared to pristine **PzPy**. The photodetector with **PzPy**/SWNT instead has a 1.9-, 3.5-, and 5.7-fold increase at 0.2, 0.6, and 1.0 V, respectively, with respect to pristine **PzPy**. Under chopped 1 Sun illumination, the **PzPy**/GNF device shows a photocurrent around 2.5 μA at 1 V of applied DC bias.

The photodetectors show a flat spectral responsivity over all the 400–750 nm visible range, with a 4- to 5-fold increase for the **PzPy**/GNF with respect to **PzPy**. The maximum response is observed toward the lowest wavelengths, reaching 0.23 and 0.80 mA W^{-1} for **PzPy** and **PzPy**/GNF-based devices, respectively. By comparison with the absorbance measurement in Figure 2, we note that the photoresponse spectrum of the **PzPy** composites has an analogous trend to the absorption one. The photocurrent is thus more intense at 400–450 nm (near to the Soret band), at 470–500 nm (in correspondence to the $n_{sulphur} \rightarrow \pi^*$ transitions), at 630–650 nm (broad $Q_y(0, 0)$ band absorption), and beyond 700 nm ($Q_x(0, 0)$ band). These observations, together with the quenching of photoluminescence (Figures 7 and 10), are a signature of photoexcited charge transfer from the **PzPy** molecule to the nanocarbons, as depicted in Figure 12b. The transferred charges are then extracted thanks to the high conductivity of the nanocarbon materials, yielding the enhanced photoresponse with respect to the bare **PzPy**.[145,146]

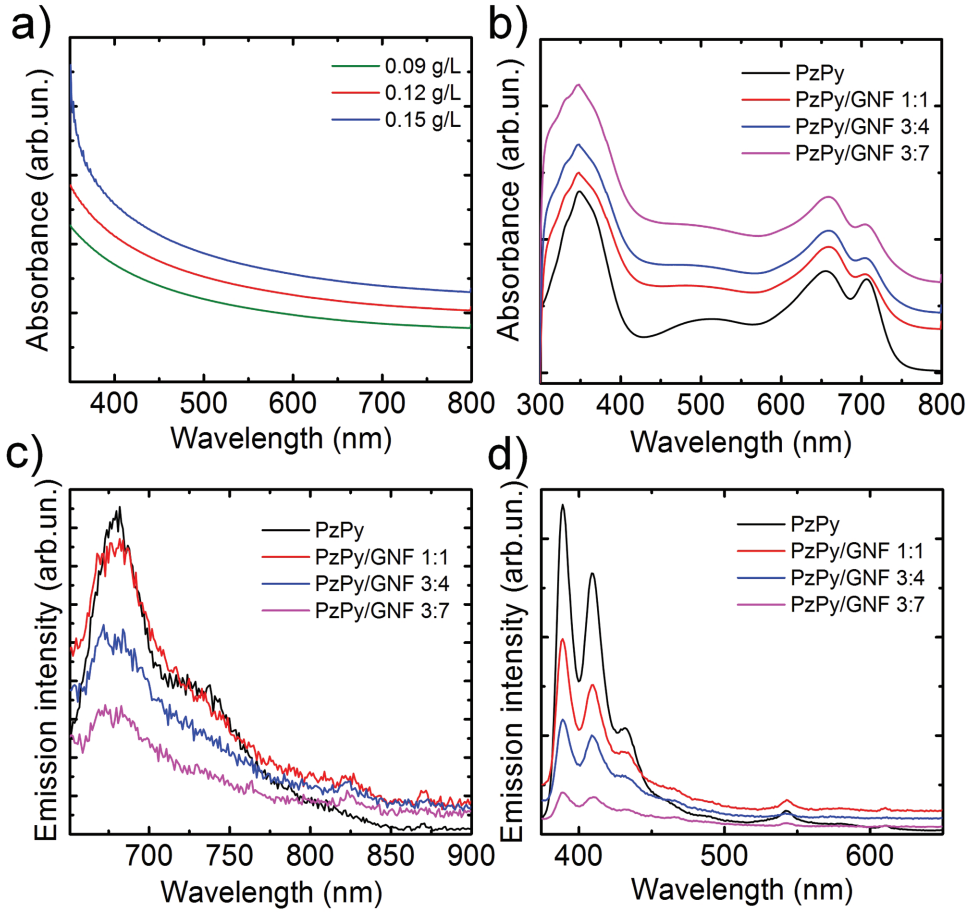

Figure 10. UV–vis absorption spectra of DMF dispersions of a) GNF and b) **PzPy**/GNF nanohybrid at various weight ratios. Emission spectra of DMF dispersions of **PzPy**/GNF nanohybrid at various weight ratios with excitation at c) 610 nm and d) 350 nm.

Transient currents under chopped 1 Sun illumination of **PzPy**/GNF are also acquired with sampling period of 0.4 s and light switching period of 5 s (**Figure 13**). After light illumination, the photocurrent is about 55% higher than before the illumination and a reversible rise/decay of the photocurrent in response to several on/off illumination cycles is observed, indicating the photocurrent stability of the nanocomposite.

From a comparison between the two types of nanocarbons used, it appears that the **PzPy**/GNF device has in general a slightly lower photoresponse than the **PzPy**/SWNT one (0.71 vs 0.78 mA W^{-1} at 500 nm). This can be explained considering the favored π–π interactions occurring between the SWNTs and the aromatic units of the **PzPy**, as previously discussed and modeled in Figure 11. However, in our view, such a small difference in performance is strongly offset by a much greater flexibility in production, and processing that GNFs offer in comparison to the SWNTs. The GNFs are easier and more economic when produced by liquid-phase exfoliation (LPE) even in large volumes,[138,147] whereas SWNTs are costly ($1000 g^{-1})[148] and the production is cumbersome, requiring further steps of purification and sorting[136,149,150] to isolate the batch of nanotubes with the desired properties. Therefore, a proof of principle of the capability of graphene to act as electron acceptor and charge transport component in **PzPy**-based photoactive nanohybrids is significant. Although these nanohybrids do not match the photocurrent values obtained by devices based on high-quality CVD graphene,[151,152] or fully optimized organic detectors,[153] the results are very promising if compared with the ones obtained by other solution-processed photoconductors attaining photocurrents on the order of 10^{-4} and 10^{-2} mA W^{-1}.[154,155]

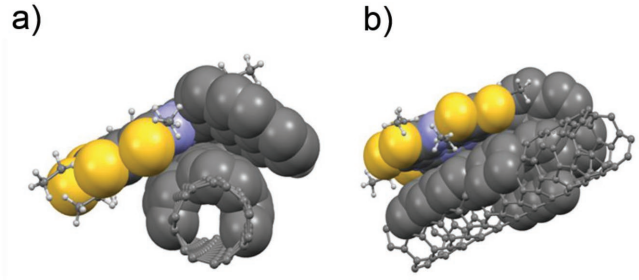

Figure 11. Molecular models of the **PzPy**/SWNT nanohybrid.

3. Conclusions

Noncovalent bonded nanohybrids composed by the novel pyrene-substituted thioethyl-porphyrazine **PzPy** and SWNTs or GNFs have been synthesized and used for photocurrent generation. The **PzPy** structure has been specifically designed to

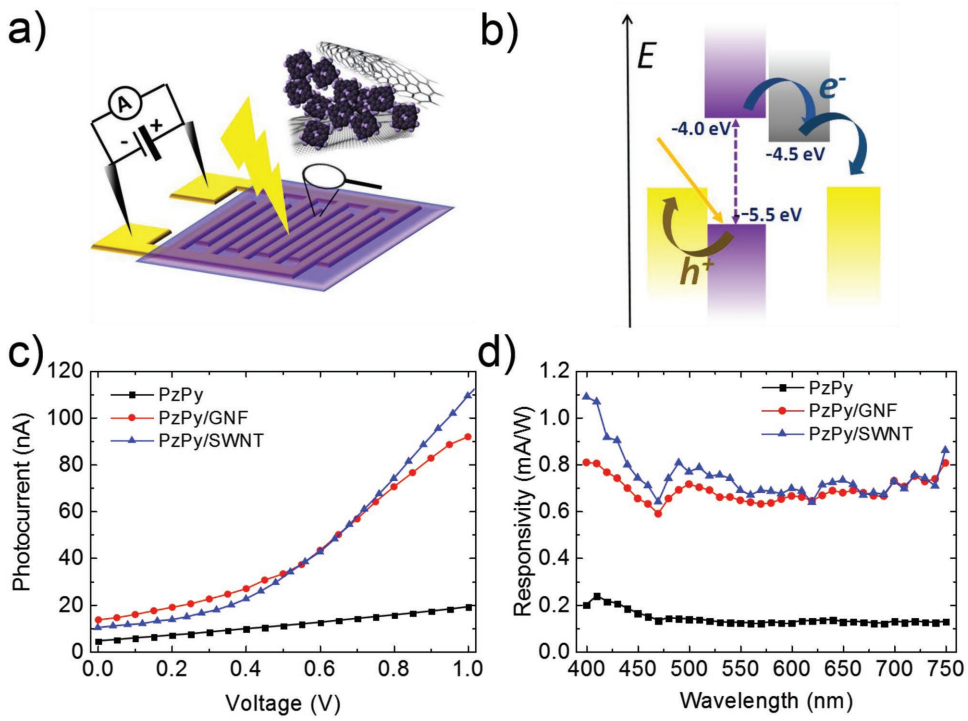

Figure 12. a) Sketch of device architecture and film composition. Interdigitated area: 0.5×0.5 cm^2. Material mass loading of the active film: 10 µg cm^{-2}. b) Energy level diagram of the materials and photodetector working principle, showing excitation by light in **PzPy** followed by electron transfer to the nanocarbon acceptor and hole transfer to the metal electrode. c) Photocurrent in **PzPy** and **PzPy** nanohybrids under 500 nm light. d) Spectral responsivity in **PzPy** and **PzPy** nanohybrids measured at 1 V.

finely tune the structural and electronic properties in order to i) promote the noncovalent interactions with π-conjugated nanocarbons, ii) enhance the spectral absorption in the visible range, iii) provide charge separation upon excitation, and iv) obtain HOMO/LUMO energy values and bandgap suitable to fit the requirements of donor materials. In particular, the thioalkyl-porphyrazine core guarantees an intense absorption in the 300–800 nm range and the presence of a pyrene moiety promotes π–π attractive interactions with the nanocarbons. In **PzPy**, the hindered rotation between the arene–arene bond gives rise to a twist of the pyrene moiety from the porphyrazine plane and, eventually, to chirality due to atropisomerism. This is an important structural feature of **PzPy** given that molecular chirality, which is a key factor in supramolecular interactions[156] and organic optoelectronics,[157] is now emerging as a relevant issue also for the development of photoactive materials.[158–160] The presence of an axially chiral structure in **PzPy** could in fact favor the interaction with semiconducting chiral nanotubes. Spectroscopic and electrochemical measurements together with TDDFT calculations provide an HOMO–LUMO energy bandgap of 1.55 eV, which makes **PzPy** suitable as absorber donor coupled with nanocarbons acceptors. Calculations show that HOMO and LUMO are localized on the pyrene and the macrocycle moiety, respectively. This gives rise to a charge separation upon HOMO–LUMO excitation, eventually preventing charge recombination. SEM and TEM analyses elucidated that in both hybrids the nanocarbons surface appeared covered by a **PzPy** film and SWNTs debundling is observed in the **PzPy**/SWNT composite. This is a clear signature that π–π interactions between **PzPy** and the SWNT sidewalls overcome nanotube–nanotube van der Waals attraction. Emission spectroscopy experiments have also shown a quench of **PzPy** fluorescence upon addition of both SWNTs and GNFs, demonstrating the occurrence of energy transfer processes. Measurements of the **PzPy**/SWNT and **PzPy**/GNF nanocomposites photoconductivity under visible light illumination have shown a higher photocurrent generation for both **PzPy**/SWNT- and

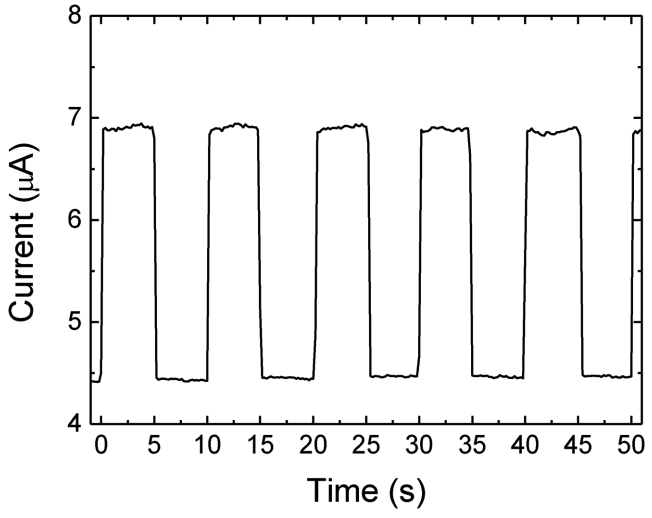

Figure 13. **PzPy**/GNF current response (at 1 V bias) to on/off cycles under 1 Sun illumination.

PzPy/GNF-based devices with respect to the one of pristine **PzPy**. Moreover, the devices based on the hybrids **PzPy**/nanocarbons have shown a spectral photoresponse 4- to 5-fold higher than **PzPy** and peaked in agreement to the **PzPy** absorption features. This confirms the presence of photoexcited charge transfer from the **PzPy** molecule to the nanocarbons. Although the **PzPy**/GNF device has a slightly lower photoresponse than the **PzPy**/SWNT one, graphene presents several advantages over SWNTs, in term of cost, preparation, processability, and environmental compatibility. The presented results open the way to the use of such hybrid materials in devices such as photodiodes and solar cells, even on flexible substrates.

4. Experimental Section

General: Chemicals and solvents were of reagent grade (Aldrich). Solvents were dried and distilled before use according to standard procedures. Solvents used in physical measurements were of spectroscopic or HPLC grade. Silica gel used for chromatography was Merck Kieselgel 60 (70–230 mesh). Commercially available SWNTs (carbon ≈90%, >77% as SWNT, $0.7 < d < 1.1$ nm) (Aldrich, code no. 704121) were used for the nanohybrid preparation after structural characterization as reported in the Supporting Information. Non-anhydrous spectroscopic grade DMF was used as solvent for the preparation of the composites of **PzPy** with SWNTs and GNFs. ^{1}H-NMR spectra were recorded on a 400, 500, or 600 MHz Varian spectrometer with $SiMe_4$ as internal standard. IR spectra were recorded using KBr disks on a JASCO J460 FT-IR spectrometer. Mass spectra were acquired in positive reflectron mode at 20 kV using Ettan MALDI-TOF Pro mass spectrometer (Amersham Biosciences) equipped with a UV nitrogen laser (337 nm) with delayed extraction mode and low mass rejection. For each spectrum 256 single shots were accumulated. Spectra were externally calibrated using two standard peptides (ile-Ang III, M+H 897.531 and hACTH 18-39, M+H 2465.199, monoisotopics). The matrix was prepared by mixing 1% w/v alpha-cyano-4-hydroxy-cinnamic acid solution, 50% acetonitrile v/v, and 0.5% v/v trifluoroacetic acid. Samples for mass spectrometric analysis were prepared by dissolving 4 µL of porphyrazine solution (<10^{-4} M in CH_2Cl_2) directly in 4 µL of the matrix. 0.4 µL of this mixture was deposited on the probe tip and allowed to evaporate. The "free-base" thioethyl porphyrazine **1**,[92] its nonsymmetrically H-substituted counterpart **2**,[81] and the Br-substituted porphyrazines **3**[82,83] are prepared according to previously described procedures.[77,78,161]

*2-(1-Pyrene)-3,7,8,12,13,17,18-heptakis(ethylthio)-5,10,15,20-21H,23H-porphyrazine (**PzPy**)*: Brominated porphyrazine **3** (100 mg, 0.123 mmol) was dissolved in a dry DMF/toluene (2:3, v/v) mixture (20 mL) heating at 100 °C under N_2. Then, potassium carbonate (136 mg, 0.984 mmol), tetrakis(triphenylphosphine) palladium(0) (10% mol, 14.0 mg, 0.0123 mmol), and 1-pyrene boronic acid (121 mg, 0.492 mmol) were added in sequence and the mixture was heated at reflux. The reaction was monitored by thin-layer chromatography and stopped after 8 h. After cooling to room temperature water (30 mL) was added and the solution was extracted with $CHCl_3$ (35 mL). The organic fractions were collected, dried over anhydrous Na_2SO_4, and filtered. After removal of the solvent under reduced pressure, the crude product was purified by column chromatography on silica gel (hexane:CH_2Cl_2 6:4 v/v), recovering **PzPy** as a dark blue solid (R_f = 0.19, 45% yield). ^{1}H-NMR (600 MHz, $CDCl_3$) δ/ppm: –1.10 (s, 2H, N_p-*H*); 0.51 (t, J = 7.4 Hz, 3H); 1.25 (t, J = 7.4 Hz, 3H); 1.44 (t, J = 7.4 Hz, 3H); 1.54 (t, J = 7.4 Hz, 3H); 1.58 (t, J = 7.4 Hz, 6H); 1.66 (t, J = 7.4 Hz, 3H); 3.06 (dq, J = 12.5, 7.4 Hz, 1H); 3.20 (dq, J = 12.5, 7.4 Hz, 1H); 3.29 (dq, J = 12.5, 7.4 Hz, 1H); 3.33 (dq, J = 12.5, 7.4 Hz, 1H); 3.91(dq, J = 7.4, 1.7 Hz, 2H); 4.13 (m, 6H); 4.29 (dq, J = 7.4, 2.6 Hz, 2H); 7.97 (d, J = 9.0 Hz, 1H); 8.07 (t, J = 7.5 Hz, 1H); 8.09 (d, J = 9.0 Hz, 1H); 8.19 (d, J = 7.5 Hz, 1H); 8.27 (d, J = 9.0 Hz, 1H); 8.31 (d, J = 9.0 Hz, 1H); 8.32 (d, J = 7.5 Hz, 1H); 8.51 (d, J = 7.5 Hz, 1H); 8.61 (d, J = 7.5 Hz, 1H). ^{13}C-NMR (125 MHz, $CDCl_3$) δ/ppm: 14.13, 14.30, 15.10, 15.64, 15.70, 15.72, 15.79, 27.84, 27.88, 29.51, 29.53, 29.61, 29.67, 29.71, 124.35, 124.76, 124.82, 125.46, 125.60, 126.13, 126.26, 127.59, 127.92, 128.16, 128.97, 130.10, 131.00, 131.01, 131.46, 131.69, 135.43, 138.97, 140.42, 140.66, 140.86, 140.90, 142.64, 143.29, 146.09, 146.40, 147.85, 149.56, 149.66, 150.43, 151.39, 152.75. MALDI-MS: m/z 935.31 $[M+H]^+$ (calcd. for $C_{46}H_{47}N_8S_7$, 935.20). UV–vis, CH_2Cl_2, λ_{max}/nm (log ε): 277 (4.33), 350 (4.63) Soret, 513 (4.11), 640 (4.29) and 709 (4.42) Q bands. FTIR (KBr $\tilde{\nu}_{max}$/cm^{-1}): 3290 (w, N_pH), 3040 (w), 2959 (m), 2923 (m), 2856 (m), 1641 (br, m), 1482 (m), 1437 (m), 1375 (w), 1066 (br, s), 799 (m), 744 (m), 700 (w), 691 (w).

***PzPy** Characterization*: The ^{1}H-NMR spectra at variable temperatures were recorded with a spectrometer operating at 600 MHz. UV–vis spectra were recorded in the 250–800 nm range by UV–vis–NIR 05E Cary spectrophotometer in 1 cm path length quartz cells (the concentration of the dispersions was ≈10^{-6} M in compound). The cyclic voltammetry and differential pulse voltammetry experiments were performed with an EG & G Princeton Applied Research Model 263A Potentiostat/Galvanostat. Data were collected and analyzed by the Model 270 electrochemical analysis system software on a PC computer.[162] A standard three-electrode arrangement was used. The working electrode was a glassy carbon button (∅ = 3 mm). A platinum wire served as a counter electrode and a home-made AgCl/Ag electrode containing saturated KCl was used as the reference electrode. All the oxidation and reduction potentials were reported relative to the ferrocene/ferrocenium (Fc/Fc^+) potential scale, using the voltammetric oxidation of Fc as an internal reference. The reproducibility of individual potential values was within ±5 mV. All the electrochemical measurements were carried out using Schlenk techniques (N_2) at room temperature. The concentration of the supporting electrolyte $[N(C_4H_9\text{-}n)_4BF_4]$ is typically of 0.15 M. Cyclic voltammograms were recorded by scanning the potential at 200 mV s^{-1}. DPV measurements were performed at 5 mV s^{-1} with a pulse height of 50 mV and a pulse width of 50 ms.

Computational Method: The Gaussian 09, Revision D.01 software,[163] was used for all the computations. The DFT using the M06 metahybrid xc functional[164] with the 6-311G(d,p) basis set as implemented in the program[165,166] was used for geometry optimization and computation of the Kohn–Sham orbital energies simulating the solvation effects by self-consistent reaction field (SCRF) integral equation formalism polarizable continuum model (IEFPCM) as implemented in the program.[105,106] Default gradient and displacement thresholds were used for the geometry optimization convergence criteria. In calculations of **PzPy** it was assumed that the thioethyl side chains conformation are similar to that already found in similar heptakis-substituted porphyrazines.[83] All the reported geometries were relative minima of the molecular potential energy surface (electronic energy in the Born–Oppenheimer approximation), as confirmed by the analytical computation of the Hessian matrix at the same level of approximation. The TDDFT[167,168] was applied for computing the excitation wavelengths, oscillator strengths, and associated excited state composition in terms of monoelectronic excitations between occupied and unoccupied Kohn–Sham orbitals at the level of theory. The Gaussian 09 default approach was used for these computations.[169] The Kohn–Sham orbitals were drawn using the program MolDen 4.9.[170] Molecular orbital isosurfaces refer to wavefunction computed at 0.02 (e au^{-3})$^{1/2}$.

Nanohybrid Preparation: (**1**) **PzPy/SWNT**: SWNTs (Sigma SWNT: carbon ≈ 90%, >77% as SWCNT, $0.7 < d < 1.1$ nm) were dispersed in DMF to make three dispersions with different initial concentrations (0.1, 0.2, and 0.4 mg mL^{-1}, respectively). The dispersions were ultrasonicated for 1 h in ice water and then centrifuged at 1500 × g for 1 h. 1 mL of the supernatant of each dispersion was taken (named C_1, C_2, and C_3, respectively). A **PzPy** solution in DMF with a concentration of 0.03 mg mL^{-1} (c = 3.21 × 10^{-5} M) was prepared (named P1). Three **PzPy**/SWNT nanocomposites at different weight ratios were prepared by mixing 3 mL of **PzPy** solution with 1 mL of C_1, C_2, and C_3, respectively. The composites (named PC_1, PC_2, and PC_3) were stirred for 10 h and then sonicated 1 min before device fabrication. The three solutions contained the same **PzPy** concentration of 0.0225 mg mL^{-1}

($c = 2.41 \times 10^{-5}$ M). (**2**) **PzPy/GNF**: Graphene nanoflakes were produced by liquid phase exfoliation of graphite.[133] Graphite flakes (1 g) (Sigma Aldrich) was dispersed in 100 mL of DMF and ultrasonicated (Branson 5800) for 6 h. The obtained dispersion was ultracentrifuged at 12 300 × *g* (in a Beckman Coulter Optima XE-90 with an SW41Ti rotor) for 30 min at 15 °C, exploiting sedimentation-based separation to remove thick flakes and unexfoliated graphite.[171,172] After the ultracentrifugation process, we collected the supernatant by pipetting. Composites are prepared by mixing graphene flakes with **PzPy** in DMF at different weight ratios and stirring for 1 d. Three composites with **PzPy**/GNF weight ratios of 1:1, 3:4, and 3:7, respectively, were produced. The three solutions contained the same **PzPy** concentration.

Nanohybrid Characterization: The SWNTs and GNFs dispersions as well as the nanohybrids were characterized by optical absorption spectroscopy in the range 300–800 nm with a Cary Varian 6000i UV–vis–NIR spectrometer. The absorption spectra were acquired using a 1 mL quartz glass cuvette. The solvent baseline is subtracted to the recorded spectrum. Photoluminescence emission spectra of the nanohybrids were recorded with a Horiba FluoroMax4 fluorimeter with excitation at 350 and 610 nm. Raman measurements were collected with a Renishaw inVia confocal Raman microscope with excitation line of 532 nm (2.33 eV) with a 50× objective lens and an incident power of ≈1 mW on the samples. The GNF and SWNT dispersions were drop cast onto Si/SiO_2 wafer (300 nm thermally grown SiO_2, LDB Technologies Ltd.) and dried under vacuum. 20 spectra were collected for each sample; Lorentzian functions were used to fit the peaks. GNFs and SWNTs were characterized morphologically by transmission electron microscopy (operated at 100 kV, JOEL JEM 1011). The materials were dropped with a pipette on holey carbon 200 mesh grids and dried under vacuum overnight. Field-emission scanning electron microscopy was also performed on samples drop cast onto Si wafer (JoelJSM-7500FA).

Device Fabrication and Measurement: Interdigitated gold electrodes were fabricated on Si/SiO_2 substrates by UV lithography with an SUSS MicroTec MJB4 mask aligner. The lithography and development of the positive photoresist were followed by thermal evaporation of chromium/gold (thickness 9 nm/40 nm) and lift off. 20 µL **PzPy** or **PzPy**/GNF (weight ratio of 1:1.3), 0.5 mg mL^{-1} chlorobenzene dispersions or **PzPy**/SWNT (weight ratio of 1:1.3), 0.5 mg mL^{-1} DMF dispersion, were drop cast on gold electrodes. Finally, the devices were annealed at 70 °C for 30 min under inert atmosphere. Photodetection experiments were performed under ambient conditions. Monochromatic light was obtained from a xenon lamp coupled to a monochromator (Spectral Products CM110) and brought to the sample with a system of lenses and mirrors in order to illuminate the device area. In this condition, the spectral responsivity was simply calculated as the ratio between the measured photocurrent density and the optical input power density for each light wavelength. Light power was measured using a calibrated Si photodiode (Thorlabs S120VC). DC bias and current measure were provided by a Keithley 2612 sourcemeter. Light was modulated with a mechanical chopper, and AC photocurrent was acquired using a current preamplifier (DL 1211) and lock-in amplifier (Signal Recovery 7265). Spectral responsivity and *IV* curves of the photodetectors were acquired at 857 Hz. The detection limit of the measurement setup was equal to 1 nA.

Transient currents under chopped 1 Sun illumination (xenon light source equipped with AM 1.5 G filters) were acquired with a sampling period of 0.4 s and a light switching period of 5 s.

Supporting Information

Supporting Information is available from the Wiley Online Library or from the author.

Acknowledgements

This project was funded by the European Union's Horizon 2020 research and innovation program under grant agreement no. 696656 (GrapheneCore1) and by Regione Basilicata under "Basilicata Innovazione" grant (Project J41H12000070001). Figure 7 was updated on May 24, 2018, following initial publication in early view.

Conflict of Interest

The authors declare no conflict of interest.

Keywords

carbon nanotubes, graphene, nanocomposites, organic photovoltaics, photocurrent, porphyrazines, supramolecular interactions, tetrapyrroles

Received: September 19, 2017
Revised: February 21, 2018
Published online: April 16, 2018

[1] *Organic Photovoltaics: Mechanisms, Materials, and Devices* (Eds: S.-S. Sun, N. S. Sariciftci), Taylor & Francis, Boca Raton, FL **2005**.
[2] C. Brabec, U. Scherf, V. Dyakonov, *Organic Photovoltaics: Materials, Device Physics, and Manufacturing Technologies*, 2nd ed., Wiley-VCH, Weinheim, Germany **2014**.
[3] B. P. Rand, H. Richter, *Organic Solar Cells: Fundamentals, Devices, and Upscaling*, Pan Stanford Publishing, CRC Press, Boca Raton, FL **2014**.
[4] B. Kippelen, J. -L. Brédas, *Energy Environ. Sci.* **2009**, *2*, 251.
[5] K. A. Mazzio, C. K. Luscombe, *Chem. Soc. Rev.* **2015**, *44*, 78.
[6] G. Yu, J. Gao, J. C. Hummelen, F. Wudl, A. J. Heeger, *Science* **1995**, *270*, 1789.
[7] J. J. M. Halls, C. A. Walsh, N. C. Greenham, E. A. Marseglia, R. H. Friend, S. C. Moratti, A. B. Holmes, *Nature* **1995**, *376*, 498.
[8] P. Schilinsky, C. Waldauf, C. J. Brabec, *Appl. Phys. Lett.* **2002**, *81*, 3885.
[9] Y. Sun, G. C. Welch, W. L. Leong, C. J. Takacs, G. C. Bazan, A. J. Heeger, *Nat. Mater.* **2012**, *11*, 44.
[10] A. Mishra, P. Baüerle, *Angew. Chem., Int. Ed.* **2012**, *51*, 2020.
[11] D. Jariwala, V. K. Sangwan, L. J. Lauhon, T. J. Marks, M. C. Hersam, *Chem. Soc. Rev.* **2013**, *42*, 2824.
[12] Y. He, Y. Li, *Phys. Chem. Chem. Phys.* **2011**, *13*, 1970.
[13] S. Cataldo, P. Salice, E. Menna, B. Pignataro, *Energy Environ. Sci.* **2012**, *5*, 5919.
[14] L. Wang, H. Liu, R. M. Konik, J. A. Misewich, S. S. Wong, *Chem. Soc. Rev.* **2013**, *42*, 8134.
[15] V. Sgobba, D. M. Guldi, *Chem. Soc. Rev.* **2009**, *38*, 165.
[16] A. C. Ferrari, F. Bonaccorso, V. Fal'ko, K. S. Novoselov, S. Roche, P. Bøggild, S. Borini, F. H. L. Koppens, V. Palermo, N. Pugno, J. A. Garrido, R. Sordan, A. Bianco, L. Ballerini, M. Prato, E. Lidorikis, J. Kivioja, C. Marinelli, T. Ryhänen, A. Morpurgo, J. N. Coleman, V. Nicolosi, L. Colombo, A. Fert, M. Garcia-Hernandez, A. Bachtold, G. F. Schneider, F. Guinea, C. Dekker, M. Barbone, Z. Sun, C. Galiotis, A. N. Grigorenko, G. Konstantatos, A. Kis, M. Katsnelson, L. Vandersypen, A. Loiseau, V. Morandi, D. Neumaier, E. Treossi, V. Pellegrini, M. Polini, A. Tredicucci, G. M. Williams, B. H. Hong, J. H. Ahn, J. M. Kim, H. Zirath, B. J. van Wees, H. van der Zant, L. Occhipinti, A. Di Matteo, I. A. Kinloch, T. Seyller, E. Quesnel, X. Feng, K. Teo, N. Rupesinghe, P. Hakonen, S. R. Neil, Q. Tannock, T. Löfwander, J. Kinaret, *Nanoscale* **2015**, *7*, 4598.
[17] X. Wan, G. Long, L. Huang, Y. Chen, *Adv. Mater.* **2011**, *23*, 5342.
[18] I. V. Lightcap, P. V. Kamat, *Acc. Chem. Res.* **2013**, *46*, 2235.
[19] D. M. Guldi, V. Sgobba, *Chem. Commun.* **2011**, *47*, 606.
[20] P. V. Kamat, *J. Phys. Chem. Lett.* **2011**, *2*, 242.

[21] F. Bonaccorso, N. Balis, M. M. Stylianakis, M. Savarese, C. Adamo, M. Gemmi, V. Pellegrini, E. Stratakis, E. Kymakis, *Adv. Funct. Mater.* **2015**, *25*, 3870.
[22] F. Bonaccorso, L. Colombo, G. Yu, M. Stoller, V. Tozzini, A. C. Ferrari, R. S. Ruoff, V. Pellegrini, *Science* **2015**, *347*, 1246501.
[23] H.-J. Choi, S.-M. Junga, J.-M. Seo, D. W. Chang, L. Dai, J.-B. Baek, *Nano Energy* **2012**, *1*, 534.
[24] M. Pumera, *Chem. Rec.* **2009**, *9*, 211.
[25] R. R. Nair, P. Blake, A. N. Grigorenko, K. S. Novoselov, T. J. Booth, T. Stauber, N. M. R. Peres, A. K. Geim, *Science* **2008**, *320*, 1308.
[26] J.-H. Kim, J. H. Hwang, J. Suh, S. Tongay, S. Kwon, C. C. Hwang, J. Wu, J. Y. Park, *Appl. Phys. Lett.* **2013**, *103*, 171604.
[27] Q. Liu, Z. Liu, X. Zhang, L. Yang, N. Zhang, G. Pan, G. S. Yin, Y. Chen, J. Wei, *Adv. Funct. Mater.* **2009**, *19*, 894.
[28] Z. Liu, Q. Liu, Y. Huang, Y. Ma, S. Yin, X. Zhang, W. Sun, Y. Chen, *Adv. Mater.* **2008**, *20*, 3924.
[29] M. G. Walter, A. B. Rudine, C. C. Wamser, *J. Porphyrins Phthalocyanines* **2010**, *14*, 759.
[30] G. Bottari, G. de la Torre, D. M. Guldi, T. Torres, *Chem. Rev.* **2010**, *110*, 6768.
[31] C. W. Tang, *Appl. Phys. Lett.* **1986**, *48*, 183.
[32] P. Peumans, S. R. Forrest, *Appl. Phys. Lett.* **2001**, *79*, 126.
[33] R. F. Bailey-Salzman, B. P. Rand, S. R. Forrest, *Appl. Phys. Lett.* **2007**, *91*, 013508.
[34] I. Kim, H. M. Haverinen, Z. Wang, S. Madakuni, Y. Kim, J. Li, G. E. Jabbour, *Chem. Mater.* **2009**, *21*, 4256.
[35] K. Takahashi, T. Goda, T. Yamaguchi, T. Komura, K. Murata, *J. Phys. Chem. B* **1999**, *103*, 4868.
[36] M. R. Axet, O. Dechy-Cabaret, J. Durand, M. Gouygou, P. Serp, *Coord. Chem. Rev.* **2016**, *308*, 236.
[37] G. Bottari, G. de la Torre, T. Torres, *Acc. Chem. Res.* **2015**, *48*, 900.
[38] D. Baskaran, J. W. Mays, X. P. Zhang, M. S. Bratcher, *J. Am. Chem. Soc.* **2005**, *127*, 6916.
[39] D. He, Y. Peng, H. Yang, D. Ma, Y. Wang, K. Chen, P. Chen, J. Shi, *Dyes Pigm.* **2013**, *99*, 395.
[40] M. E. Lipińska, S. L. H. Rebelo, M. F. R. Pereira, J. L. Figueiredo, C. Freire, *Mater. Chem. Phys.* **2013**, *143*, 296.
[41] B. Ballesteros, S. Campidelli, G. de la Torre, C. Ehli, D. M. Guldi, M. Prato, T. Torres, *Chem. Commun.* **2007**, *28*, 2950.
[42] B. Ballesteros, G. de la Torre, C. Ehli, G. M. A. Rahman, F. Agulló-Rueda, D. M. Guldi, T. Torres, *J. Am. Chem. Soc.* **2007**, *129*, 5061.
[43] S. Campidelli, B. Ballesteros, A. Filoramo, D. Diaz Díaz, G. de la Torre, T. Torres, G. M. A. Rahman, C. Ehli, D. Kiessling, F. Werner, V. Sgobba, D. M. Guldi, C. Cioffi, M. Prato, J. P. Bourgoin, *J. Am. Chem. Soc.* **2008**, *130*, 11503.
[44] K. Qu, H. Xu, C. Zhao, J. Ren, X. Qu, *RSC Adv.* **2011**, *1*, 632.
[45] D. M. Guldi, G. M. A. Rahman, S. Quin, M. Tchoul, W. T. Ford, M. Marcaccio, D. Paolucci, F. Paolucci, S. Campidelli, M. Prato, *Chem. Eur. J.* **2006**, *12*, 2152.
[46] S. K. Das, N.. K. Subbaiyan, F. D'Souza, A. S. D. Sandanayaka, T. Hasobe, O. Ito, *Energy Environ. Sci.* **2011**, *4*, 707.
[47] R. Chitta, A. S. D. Sandanayaka, A. L. Schumacher, L. D'Souza, Y. Araki, O. Ito, F. D'Souza, *J. Phys. Chem. C* **2007**, *111*, 6947.
[48] D. M. Guldi, G. M. A. Rahman, M. Prato, N. Jux, S. Qin, W. Ford, *Angew. Chem., Int. Ed.* **2005**, *44*, 2015.
[49] V. Sgobba, G. M. A. Rahman, D. M. Guldi, N. Jux, S. Campidelli, M. Prato, *Adv. Mater.* **2006**, *18*, 2264.
[50] T. Hasobe, S. Fukuzumi, P. V. Kamat, *J. Phys. Chem. B* **2006**, *110*, 25477.
[51] J. Bartelmess, A. R. M. Soares, M. V. Martinez-Diaz, M. G. P. M. S. Neves, A. C. Tomé, J. A. S. Cavaleiro, T. Torres, D. M. Guldi, *Chem. Comm.* **2011**, *47*, 3490.
[52] E. Maligaspe, A. S. D. Sandanayaka, T. Hasobe, O. Ito, F. D'Souza, *J. Am. Chem. Soc.* **2010**, *132*, 8158.
[53] H. Murakami, T. Nomura, N. Nakashima, *Chem. Phys. Lett.* **2003**, *378*, 481.
[54] S. Kyatskaya, J. R. G. Mascaros, L. Bogani, F. Hennrich, M. Kappes, W. Wernsdorfer, M. Ruben, *J. Am. Chem. Soc.* **2009**, *131*, 15143.
[55] J. Bartelmess, B. Ballesteros, G. de la Torre, D. Kiessling, S. Campidelli, M. Prato, T. Torres, D. M. Guldi, *J. Am. Chem. Soc.* **2010**, *132*, 16202.
[56] M. Ince, J. Bartelmess, D. Kiessling, K. Dirian, M. V. Martínez-Díaz, T. Torres, D. M. Guldi, *Chem. Sci.* **2012**, *3*, 1472.
[57] R. A. Hatton, N. P. Blanchard, V. Stolojan, A. J. Miller, S. R. P. Silva, *Langmuir* **2007**, *23*, 6424.
[58] S. K. Das, N. K. Subbaiyan, F. D'Souza, A. S. D. Sandanayaka, T. Wakahara, O. Ito, *J. Porphyrins Phthalocyanines* **2011**, *15*, 1033.
[59] A. S. D. Sandanayaka, N. K. Subbaiyan, S. K. Das, R. Chitta, E. Maligaspe, T. Hasobe, O. Ito, F. D'Souza, *ChemPhysChem* **2011**, *12*, 2266.
[60] J. Bartelmess, C. Ehli, J.-J. Cid, M. Garcia-Iglesias, P. Vazquez, T. Torres, D. M. Guldi, *Chem. Sci.* **2011**, *2*, 652.
[61] J. Bartelmess, C. Ehli, J.-J. Cid, M. Garcia-Iglesias, P. Vazquez, T. Torres, D. M. Guldi, *J. Mater. Chem.* **2011**, *21*, 8014.
[62] Q. Zhong, V. V. Diev, S. T. Roberts, P. D. Antunez, R. L. Brutchey, S. E. Bradforth, M. E. Thompson, *ACS Nano* **2013**, *7*, 3466.
[63] E. Bekyarova, S. Sarkar, F. Wang, M. E. Itkis, I. Kalinina, X. Tian, R. C. Haddon, *Acc. Chem. Res.* **2013**, *46*, 65.
[64] B. Wang, V. Engelhardt, A. Roth, R. Faust, D. M. Guldi, *Nanoscale* **2017**, *9*, 11632.
[65] A. Roth, M.-E. Ragoussi, L. Wibmer, G. Katsukis, G. de la Torre, T. Torres, D. M. Guldi, *Chem. Sci.* **2014**, *5*, 3432.
[66] C. K. C. Bikram, S. K. Das, K. Ohkubo, S. Fukuzumi, F. D'Souza, *Chem. Commun.* **2012**, *48*, 11859.
[67] M.-E. Ragoussi, G. Katsukis, A. Roth, J. Malig, G. de la Torre, D. M. Guldi, T. Torres, *J. Am. Chem. Soc.* **2014**, *136*, 4593.
[68] M.-E. Ragoussi, J. Malig, G. Katsukis, B. Butz, E. Spiecker, G. de la Torre, T. Torres, D. M. Guldi, *Angew. Chem., Int. Ed.* **2012**, *51*, 6421.
[69] J. Malig, N. Jux, D. Kiessling, J.-J. Cid, P. Vazquez, T. Torres, D. M. Guldi, *Angew. Chem., Int. Ed.* **2011**, *50*, 3561.
[70] L. Brinkhaus, G. Katsukis, J. Malig, R. D. Costa, M. Garcia-Iglesias, P. Vazquez, T. Torres, D. M. Guldi, *Small* **2013**, *9*, 2348.
[71] X. Zhang, Y. Feng, S. Tang, W. Feng, *Carbon* **2010**, *48*, 211.
[72] B. Mondal, R. Bera, S. K. Nayak, A. Patra, *J. Mater. Chem. C* **2016**, *4*, 6027.
[73] Y. Yang, R. Suna, M. Tanga, S. Rena, *Physica E* **2017**, *86*, 76.
[74] V. Georgakilas, J. N. Tiwari, K. C. Kemp, J. A. Perman, A. B. Bourlinos, K. S. Kim, R. Zboril, *Chem. Rev.* **2016**, *116*, 5464.
[75] C. C. Leznoff, A. B. P. Lever, *Phthalocyanines, Properties and Applications*, Vols. *1–4*, VCH, New York 1989–1996.
[76] P. A. Stuzhin, C. Ercolani, in *The Porphyrin Handbook, Vol 15. Phthalocyanines: Synthesis* (Eds: K. M. Kadish, K. M. Smith, R. Guilard), Academic Press, New York **2003**, pp. 263–365.
[77] F. Lelj, G. Morelli, G. Ricciardi, A. Roviello, A. Sirigu, *Liq. Cryst.* **1992**, *12*, 941.
[78] S. Belviso, G. Ricciardi, F. Lelj, *J. Mater. Chem.* **2000**, *10*, 297.
[79] S. Belviso, M. Amati, M. De Bonis, F. Lelj, *Mol. Cryst. Liq. Cryst.* **2008**, *481*, 56.
[80] S. Belviso, F. Cammarota, R. Rossano, F. Lelj, *J. Porphyrins Phthalocyanines* **2016**, *20*, 223.
[81] S. Belviso, G. Ricciardi, F. Lelj, L. Monsù Scolaro, A. Bencini, C. Carbonera, *J. Chem. Soc., Dalton Trans.* **2001**, 1143.
[82] S. Belviso, A. Giugliano, M. Amati, G. Ricciardi, F. Lelj, L. Monsù Scolaro, *Dalton Trans.* **2004**, 305.
[83] S. Belviso, M. Amati, R. Rossano, A. Crispini, F. Lelj, *Dalton Trans.* **2015**, *44*, 2191.
[84] J. Nelson, *Science* **2001**, *293*, 1059.

[85] L. Schmidt-Mende, A. Fechtenkotter, K. Mullen, E. Moons, R. H. Friend, J. D. MacKenzie, *Science* **2001**, *293*, 1119.
[86] Q. Sun, L. Dai, X. Zhou, L. Li, Q. Li, *Appl. Phys. Lett.* **2007**, *91*, 253505.
[87] J. Mack, M. J. Stillman, in *The Porphyrin Handbook, Vol 16. Phthalocyanines: Spectroscopic and Electrochemical Characterization* (Eds: K. M. Kadish, K. M. Smith, R. Guilard), Academic Press, New York **2003**, pp. 43–116.
[88] M. Gouterman, *J. Mol. Spectrosc.* **1961**, *6*, 138.
[89] M. Gouterman, in *The Porphyrins* (Ed: D. Dolphin), Vol. *3*, Academic Press, New York **1978**, pp. 1–165.
[90] G. de la Torre, P. Vázquez, F. Agulló-López, T. Torres, *Chem. Rev.* **2004**, *104*, 3723.
[91] H. Xu, R. Chen, Q. Sun, W. Lai, Q. Su, W. Huang, X. Liu, *Chem. Soc. Rev.* **2014**, *43*, 3207.
[92] G. Ricciardi, S. Belviso, F. Lelj, S. Ristori, *J. Porphyrins Phthalocyanines* **1998**, *2*, 177.
[93] N. Miyaura, A. Suzuki, *Chem. Rev.* **1995**, *95*, 2457.
[94] C. M. Muzzi, C. J. Medforth, L. Voss, M. Cancilla, C. Lebrilla, J.-G. Ma, J. A. Shelnutt, K. M. Smith, *Tetrahedron Lett.* **1999**, *40*, 6159.
[95] S. M. Kozlov, F. Vines, A. Gorling, *Carbon* **2012**, *50*, 2482.
[96] C. A. Hunter, K. R. Lawson, C. Perkins, C. J. Urch, *J. Chem. Soc., Perkin Trans. 2* **2001**, *2*, 651.
[97] X.-Q. Chen, X.-Y. Liao, J.-G. Yu, F.-P. Jiao, X.-Y. Jiang, *Nano* **2013**, *8*, 1330002.
[98] G. Liu, F. Wang, S. Chaunchaiyakul, Y. Saito, A. Bauri, T. Kimura, Y. Kuwahara, N. Komatsu, *J. Am. Chem. Soc.* **2013**, *135*, 4805.
[99] G. Liu, A. F. M. M. Rahman, S. Chaunchaiyakul, T. Kimura, Y. Kuwahara, N. Komatsu, *Chem. Eur. J.* **2013**, *19*, 16221.
[100] G. Liu, T. Yasumitsu, L. Zhao, X. Peng, F. Wang, A. K. Bauri, S. Aonuma, T. Kimura, N. Komatsu, *Org. Biomol. Chem.* **2012**, *10*, 5830.
[101] F. Wang, K. Matsuda, A. F. M. M. Rahman, T. Kimura, N. Komatsu, *Nanoscale* **2011**, *3*, 4117.
[102] X. Peng, N. Komatsu, S. Bhattacharya, T. Shimawaki, S. Aonuma, T. Kimura, A. Osuka, *Nat. Nanotechnol.* **2007**, *2*, 361.
[103] C. A. Hunter, *Chem. Soc. Rev.* **1994**, *23*, 101.
[104] S. Superchi, M. I. Donnoli, G. Proni, G. P. Spada, C. Rosini, *J. Org. Chem.* **1999**, *64*, 4762.
[105] J. Tomasi, B. Mennucci, R. Cammi, *Chem. Rev.* **2005**, *105*, 2999.
[106] G. Scalmani, M. J. Frisch, *J. Chem. Phys.* **2010**, *132*, 114110.
[107] F. Ceccacci, G. Mancini, P. Mencarelli, C. Villani, *Tetrahedron: Asymmetry* **2003**, *14*, 3117.
[108] S. Levi Mortera, R. Sabia, M. Pierini, F. Gasparrini, C. Villani, *Chem. Commun.* **2012**, *48*, 3167.
[109] R. Sabia, A. Ciogli, M. Pierini, F. Gasparrini, C. Villani, *J. Chromatogr. A* **2014**, *1362*, 144.
[110] S. Belviso, E. Santoro, F. Lelj, D. Casarini, C. Villani, R. Franzini, S. Superchi, *Eur. J. Org. Chem.* **2018**, submitted.
[111] E. L. Eliel, S. H. Wilen, L. N. Mander, *Stereochemistry of Organic Compounds*, Wiley, New York **1994**. pp. 1142–1148.
[112] M. Oki, in *Topics in Stereochemisty* (Eds: E. L. Eliel, N. L. Allinger, S. H. Wilen), Vol. *14*, John Wiley & Sons, New York **1983**, pp. 3–4.
[113] S. A. Asher, *Anal. Chem.* **1984**, *56*, 720.
[114] H. H. Jaffé, M. Orchin, *Theory and Applications of Ultraviolet Spectroscopy*, John Wiley & Sons, New York **1962**, pp. 334–335.
[115] C. Nitschke, S. M. O'Flaherty, M. Kroll, W. J. Blau, *J. Phys. Chem. B* **2004**, *108*, 1287.
[116] A. A. Esenpinar, M. Bulut, *Dyes Pigments* **2008**, *76*, 249.
[117] M. J. Stillman, T. Nyokong, in *Phthalocyanines: Properties and Applications* (Eds: C. C. Leznoff, A. B. P. Lever), VCH, Weinheim **1989**, p. 139.
[118] H. Isago, H. Fujita, *J. Porphyrins Phthalocyanines* **2013**, *17*, 447.
[119] H. Isago, *Optical Spectra of Phthalocyanines and Related Compounds*, Springer, Japan, **2015**, pp. 79–80.
[120] H. M. Grant, P. Mctigue, D. G. Ward, *Aust. J. Chem.* **1983**, *36*, 2211.
[121] *CRC Handbook of Chemistry and Physics*, 91th ed. (Ed: W. H. Haynes), CRC Press, Boca Raton, FL **2010**, pp. 8–42.
[122] W. L. F. Armarego, C. L. L. Chai, *Purification of Laboratory Chemicals*, 5th ed., Butterworth-Heinemann, Burlington, MA **2003**, pp. 215–216.
[123] L. A. Bottomley, W. H. Chiou, *J. Electroanal. Chem.* **1986**, *198*, 331.
[124] E. A. Ough, K. A. M. Creber, M. Stillman, *Inorg. Chim. Acta* **1996**, *246*, 361.
[125] The number of exchanged electrons in each of these redox processes is also confirmed by analyzing the width of the peaks at half height in the corresponding differential small pulse amplitude voltammograms. Considering that in our pulse voltammograms obtained using a pulse amplitude of 50 mV, the measured values of the peak half widths are greater than 90.4 mV, a one-electron reduction processes has to be associated with all the studied compounds. See, E. P. Perry, R. A. Osteryoung, *Anal. Chem.* **1965**, *37*, 1634.
[126] Y. Liu, M. S. Liu, X-C. Li, A. K-Y. Jen, *Chem. Mater.* **1998**, *10*, 3301.
[127] J. Pommerehne, H. Vestweber, W. Guss, R. F. Mahrt, H. Bassler, M. Porch, J. Daub, *Adv. Mater.* **1995**, *7*, 551.
[128] B. W. D. Andrade, S. Datta, S. R. Forrest, P. Djurovich, E. Polikarpov, M. E. Thompson, *Org. Electron.* **2005**, *6*, 11.
[129] R. J. Davis, M. T. Lloyd, S. R. Ferreira, M. J. Bruzek, S. E. Watkins, L. Lindell, P. Sehati, M. Fahlman, J. E. Anthony, J. W. P. Hsu, *J. Mater. Chem.* **2011**, *21*, 1721.
[130] S. Suzuki, C. Bower, Y. Watanabe, O. Zhou, *Appl. Phys. Lett.* **2000**, *76*, 4007.
[131] J. P. Sun, Z. X. Zhang, S. M. Hou, G. M. Zhang, Z. N. Gu, X. Y. Zhao, W. M. Liu, Z. Q. Xue, *Appl. Phys. A* **2002**, *75*, 479.
[132] H. Xu, R. Chen, Q. Sun, W. Lai, Q. Su, W. Huang, X. Liu, *Chem. Soc. Rev.* **2014**, *43*, 3259.
[133] Y. Hernandez, V. Nicolosi, M. Lotya, F. M. Blighe, Z. Sun, S. De, I. T. McGovern, B. Holland, M. Byrne, Y. K. Gun'Ko, J. J. Boland, P. Niraj, G. Duesberg, S. Krishnamurthy, R. Goodhue, J. Hutchison, V. Scardaci, A. C. Ferrari, J. N. Coleman, *Nat. Nanotechnol.* **2008**, *3*, 563.
[134] T. Hasan, P. H. Tan, F. Bonaccorso, A. G. Rozhin, V. Scardaci, W. I. Milne, A. C. Ferrari, *J. Phys. Chem. C* **2008**, *112*, 20227.
[135] S. Casaluci, M. Gemmi, V. Pellegrini, A. Di Carlo, F. Bonaccorso, *Nanoscale* **2016**,*8*, 5368.
[136] F. Bonaccorso, T. Hasan, P. H. Tan, C. Sciascia, G. Privitera, G. Di Marco, P. G. Gucciardi, A. C. Ferrari, *J. Phys. Chem. C* **2010**, *114*, 17267.
[137] C. Ehli, G. M. A. Rahman, N. Jux, D. Balbinot, D. M. Guldi, F. Paolucci, M. Marcaccio, D. Paolucci, M. Melle-Franco, F. Zerbetto, S. Campidelli, M. Prato, *J. Am. Chem. Soc.* **2006**, *128*, 11222.
[138] F. Bonaccorso, A. Bartolotta, J. N. Coleman, C. Backes, *Adv. Mater.* **2016**, *28*, 6136.
[139] A. C. Ferrari, J. C. Meyer, V. Scardaci, C. Casiraghi, M. Lazzeri, F. Mauri, S. Piscanec, D. Jiang, K. S. Novoselov, S. Roth, A. K. Geim, *Phys. Rev. Lett.* **2006**, *97*, 187401.
[140] A. C. Ferrari, J. Robertson, *Phys. Rev. B* **2001**, *64*, 075414.
[141] J. Hassoun, F. Bonaccorso, M. Agostini, M. Angelucci, M. G. Betti, R. Cingolani, M. Gemmi, C. Mariani, S. Panero, V. Pellegrini, B. Scrosati, *Nano Lett.* **2014**, *14*, 4901.
[142] C. Casiraghi, A. Hartschuh, H. Qian, S. Piscanec, C. Georgi, A. Fasoli, K. S. Novoselov, D. M. Basko, A. C. Ferrari, *Nano Lett.* **2009**, *9*, 1433.
[143] A. C. Ferrari, D. M. Basko, *Nat. Nanotechnol.* **2013**, *8*, 235.
[144] Z. Mo, X. Zhu, G. Wang, W. Han, R. Guo, *J. Mater. Res.* **2014**, *29*, 2156.
[145] G. Konstantatos, M. Badioli, L. Gaudreau, J. Osmond, M. Bernechea, F. P. G. de Arquer, F. Gatti, F. H. L. Koppens, *Nat. Nanotechnol.* **2012**, *7*, 363.
[146] Z. Sun, Z. Liu, J. Li, G. Tai, S.-P Lau, F. Yan, *Adv. Mater.* **2012**, *24*, 5878.

[147] F. Bonaccorso, A. Lombardo, T. Hasan, Z. Sun, L. Colombo, A. C. Ferrari, *Mater. Today* **2012**, *15*, 564.
[148] http://www.sigmaaldrich.com/catalog/product/aldrich/775533?lang=it&region=IT (accessed: April 2018).
[149] M. S. Arnold, A. A. Green, J. F. Hulvat, S. I. Stupp, M. C. Hersam, *Nature Nanotechnol.* **2006**, *1*, 60.
[150] M. S. Arnold, S. I. Stupp, M. C. Hersam, *Nano Lett.* **2005**, *5*, 713.
[151] S.-Y. Chen, Y.-Y. Lu, F.-Y. Shih, P.-H Ho, Y.-F. Chen, C.-W. Chen, Y.-T Chen, W.-H. Wang, *Carbon* **2013**, *63*, 23.
[152] For a review see F. H. L. Koppens, T. Mueller, P. Avouris, A. C. Ferrari, M. S. Vitiello, M. Polini, *Nat. Nanotechnol.* **2014**, *9*, 780.
[153] K.-J. Baeg, M. Binda, D. Natali, M. Caironi, Y.-Y. Noh, *Adv. Mater.* **2013**, *25*, 4267.
[154] D. J. Finn, M. Lotya, G. Cunningham, R. J. Smith, D. McCloskey, J. F. Donegan, J. N. Coleman, *J. Mater. Chem. C* **2014**, *2*, 925.
[155] F. Withers, H. Yang, L. Britnell, A. P. Rooney, E. Lewis, A. Felten, C. R. Woods, V. Sanchez Romaguera, T. Georgiou, A. Eckmann, Y. J. Kim, S. G. Yeates, S. J. Haigh, A. K. Geim, K. S. Novoselov, C. Casiraghi, *Nano Lett.* **2014**, *14*, 3987.
[156] *Chirality in Supramolecular Assemblies: Causes and Consequences* (Ed: F. R. Keene), Wiley, Chichester, UK **2016**.
[157] V. Tasco, M. Esposito, F. Todisco, A. Benedetti, M. Cuscunà, D. Sanvitto, A. Passaseo, *Appl. Phys. A.* **2016**, *122*, 1.
[158] K. Sugawara, N. Nakamura, Y. Yamane, S. Hayase, T. Nokami, T. Itoh, *Green Energy Environ.* **2016**, *1*, 149.
[159] C. Liu, G. Yang, Y. Si, Y. Liu, X. Pan, *J. Mater. Chem. C* **2017**, *5*, 3495.
[160] P. Josse, L. Favereau, C. Shen, S. Dabos-Seignon, P. Blanchard, C. Cabanetos, J. Crassous, *Chem. Eur. J.* **2017**, *23*, 6277.
[161] G. Ricciardi, S. Belviso, G. Giancane, R. Tafuro, T. Wagner, L. Valli, *J. Phys. Chem. B* **2004**, *108*, 7854.
[162] A. J. Bard, L. R. Faulkner, *Electrochemical Methods, Fundamentals and Applications*, John Wiley & Sons, New York **1980**.
[163] M. J. Frisch, G. W. Trucks, H. B. Schlegel, G. E. Scuseria, M. A. Robb, J. R. Cheeseman, G. Scalmani, V. Barone, B. Mennucci, G. A. Petersson, H. Nakatsuji, M. Caricato, X. Li, H. P. Hratchian, A. F. Izmaylov, J. Bloino, G. Zheng, J. L. Sonnenberg, M. Hada, M. Ehara, K. Toyota, R. Fukuda, J. Hasegawa, M. Ishida, T. Nakajima, Y. Honda, O. Kitao, H. Nakai, T. Vreven, J. A. Montgomery Jr., J. E. Peralta, F. Ogliaro, M. Bearpark, J. J. Heyd, E. Brothers, K. N. Kudin, V. N. Staroverov, R. Kobayashi, J. Normand, K. Raghavachari, A. Rendell, J. C. Burant, S. S. Iyengar, J. Tomasi, M. Cossi, N. Rega, J. M. Millam, M. Klene, J. E. Knox, J. B. Cross, V. Bakken, C. Adamo, J. Jaramillo, R. Gomperts, R. E. Stratmann, O. Yazyev, A. J. Austin, R. Cammi, C. Pomelli, J. W. Ochterski, R. L. Martin, K. Morokuma, V. G. Zakrzewski, G. A. Voth, P. Salvador, J. J. Dannenberg, S. Dapprich, A. D. Daniels, Ö. Farkas, J. B. Foresman, J. V. Ortiz, J. Cioslowski, D. J. Fox, Gaussian 09, Revision D.01. Gaussian, Inc., Wallingford, CT **2013**.
[164] Y. Zhao, D. G. Truhlar, *Theor. Chem. Acc.* **2008**, *120*, 215.
[165] J. S. Binkley, J. A. Pople, W. J. Hehre, *J. Am. Chem. Soc.* **1980**, *102*, 939.
[166] M. S. Gordon, J. S. Binkley, J. A. Pople, W. J. Pietro, W. J. Hehre, *J. Am. Chem. Soc.* **1982**, *104*, 2797.
[167] M. Casida, in *Recent Advances in Density Functional Methods* (Ed: D. P. Chong), Vol. *1*, World Scientific, Singapore **1995**, p. 155.
[168] M. E. Casida, C. Jamorski, K. C. Casida, D. R. Salahub, *J. Chem. Phys.* **1998**, *108*, 4439.
[169] R. E. Stratmann, G. E. Scuseria, M. J. Frisch, *J. Chem. Phys.* **1998**, *109*, 8218.
[170] G. Schaftenaar, J. H. Noordik, *J. Comput.-Aided Mol. Des.* **2000**, *14*, 123.
[171] A. Capasso, A. E. Del Rio Castillo, H. Sun, A. Ansaldo, V. Pellegrini, F. Bonaccorso, *Solid State Commun.* **2016**, *224*, 53.
[172] A. C. Ferrari, J. Robertson, *Phys. Rev. B* **2000**, *61*, 14095.